PERGAMON

Journal of Asian Earth Sciences 20 (2002) 459–479

Journal of Asian Earth Sciences

www.elsevier.com/locate/jseaes

Records of the evolution of the Himalayan orogen from in situ Th–Pb ion microprobe dating of monazite: Eastern Nepal and western Garhwal

E.J. Catlos[a,*], T.M. Harrison[a], C.E. Manning[b], M. Grove[b], S.M. Rai[c], M.S. Hubbard[d], B.N. Upreti[c]

[a]*Department of Earth and Space Sciences, Institute of Geophysics and Planetary Physics, University of California, Los Angeles, CA 90095-1567, USA*
[b]*Department of Earth and Space Sciences, University of California, Los Angeles, CA 90095-1567, USA*
[c]*Department of Geology, Tri-Chandra Campus, Tribhuvan University, Kathmandu, Nepal*
[d]*Department of Geology, Kansas State University, Manhattan, KS 66506, USA*

Received 8 September 2000; revised 22 March 2001; accepted 27 March 2001

Abstract

In situ Th–Pb monazite ages from rocks collected along two transects (the Dudh Kosi-Everest, eastern Nepal and the Bhagirathi River, Garhwal Himalaya, India) perpendicular to the Main Central Thrust (MCT) suggest a striking continuity of tectonic events across the Himalaya. The youngest age reported in this study, 5.9 ± 0.2 Ma (MSWD = 0.4), from matrix monazite grains collected beneath the MCT in the Garhwal region is consistent with several age data from rocks at similar structural levels in central Nepal, providing support for widespread Late Miocene MCT activity. The lateral parallelism of orogenic events is further manifested by the 20.7 ± 0.1 Ma age of a High Himalayan leucogranite from an injection complex that outcrops along the Dudh Kosi-Everest transect, resembling ages of these bodies reported elsewhere. The youngest monazite grain analyzed along the Dudh Kosi-Everest transect is 10.3 ± 0.8 Ma. The absence of 7–3 Ma monazite ages in eastern Nepal may reflect a different nappe structure, which obscures the reactivated ramp equivalent exposed in the Garhwal and central Nepal. Garnets from the MCT hanging wall (Greater Himalayan Crystallines) and footwall (Lesser Himalaya) display different major element zoning, and the patterns are useful for constraining the location of the thrust system that separates the two lithologies. Pressure–temperature paths for two upper Lesser Himalayan garnets that contain monazite inclusions indicate the utility of an in situ methodology to constrain the metamorphic evolution of the shear zone. Along the Dudh Kosi-Everest transect, upper Lesser Himalayan monazite grains from three rocks record a clear signal at 14.5 ± 0.1 Ma (MSWD = 8.4), and the ~23 Ma age that characterizes the hanging wall is notably absent. Monazites collected within a large-scale Greater Himalayan Crystallines fold yield the ~14 Ma age, consistent with the structure forming due to MCT-related compression. Paleo-Mesoproterozoic (1407 ± 35 Ma) matrix monazite grains are found within an augen gneiss unit located beneath the MCT, whereas Cambro-Ordovician (436 ± 8; 548 ± 17 Ma) inclusions are preserved within garnets of the Greater Himalayan Crystallines. The presence of 45.2 ± 2.1 Ma grains from lower structural levels of the Greater Himalayan Crystallines indicates the unit realized conditions conducive for monazite growth during the Eocene.

Keywords: Himalaya; Monazite; Main Central Thrust; Metamorphism; Geochronology

1. Introduction

Nineteenth century geologists studying the Himalaya perceived an anomalous geologic relationship that appeared to contradict two commonly accepted principles: that the oldest rocks in a sedimentary succession are found at the base of the pile, and that metamorphosed strata are older than unmetamorphosed. The Main Central Thrust (MCT), located at the foot of the Himalayas, places lower-grade Lesser Himalayan metasediments beneath the high-grade gneisses of the Greater Himalayan Crystallines. Exploration of the Himal Pradesh region, northern India, surprised the pioneering geologists (Medicott, 1864; Oldham, 1883; Middlemiss, 1887), who saw the highest-grade, and thus supposedly oldest rocks, form the tallest peaks. The recognition of widespread thrusting within the Himalaya was largely based on their observations (Pilgrim and West, 1928; Auden, 1937), and the orogen's 'inverted metamorphism,' an increase in metamorphic intensity towards higher structural levels, appeared resolved by invoking tectonic activity.

However, subsequent detailed studies suggested that the MCT footwall is characterized by an apparent inverted

* Corresponding author. Tel.: +1-310-206-2940; fax: +1-310-825-2779.
E-mail address: catlog@argon.ess.ucla.edu (E.J. Catlos).

1367-9120/02/$ - see front matter
PII: S1367-9120(01)00039-6

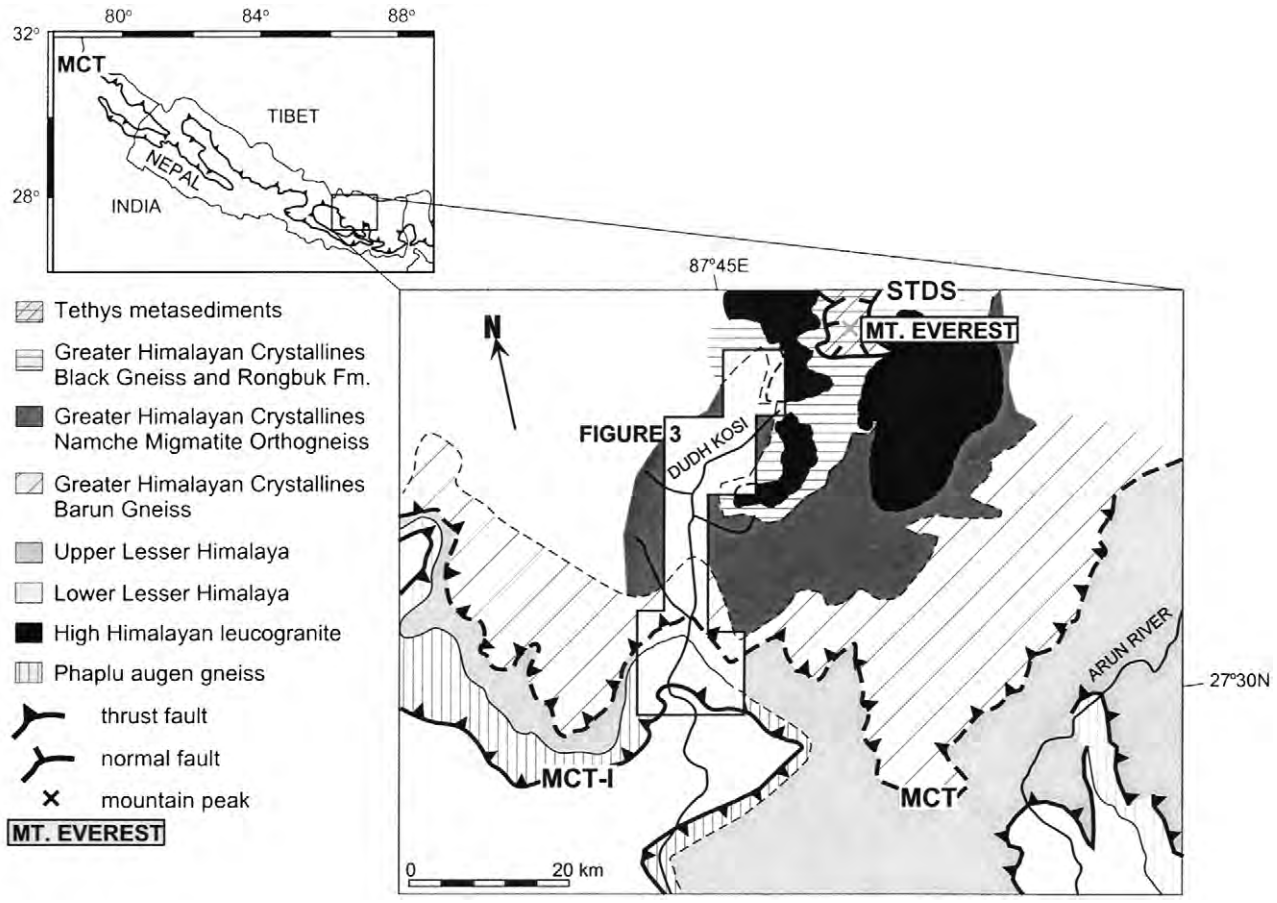

Fig. 1. Generalized geologic map of eastern Nepal after Akiba et al. (1973), Carosi et al. (1996b), Lombardo et al. (1993), and our field interpretations. The upper left inset shows the location of the Dudh Kosi-Everest area in context of country borders and the approximate lateral extent of the MCT. See Le Fort (1996), Harrison et al. (1999a), or Hodges (2000) for detailed geologic maps of the Himalaya and southern Tibet. The Dudh Kosi drainage is outlined in Fig. 3.

geotherm (Ray, 1947; Gansser, 1964; Pêcher, 1989; England et al., 1992). The idea of Himalayan inverted metamorphism reemerged, but was, to a greater degree, relocated to the MCT footwall. This type of metamorphism is typically associated with areas of extensive thrust faulting (Ernst, 1973; Graham and England, 1976; Spear et al., 1995), where heat is thought to redistribute from a hot upper plate to a colder lower plate (e.g., Le Fort, 1975). Several models aimed at expanding our perception of processes that could develop such thermal structure in areas of thickened continental crust have been proposed (Le Fort, 1975; Searle and Rex, 1989; England et al., 1992; Hubbard, 1996; Huerta et al., 1996; Harrison et al., 1998), but whether they apply to the Himalaya remains debatable (Harrison et al., 1999a; Hodges, 2000). Understanding the origin of this phenomenon has implications for establishing the role of various crustal heat sources (e.g., radiogenic, asthenospheric input, shear heating, addition of melts) and mechanisms of heat transfer within collisional belts. Thus, obtaining time constraints on the deformation events recorded within the Himalaya remains key to deciphering its evolution.

Monazite is a common Th-bearing accessory mineral found in the metapelitic lithologies that dominate Himalayan metamorphic sequences and is speculated to form under conditions coincident with the garnet isograd (~525°C; Smith and Barreiro, 1990). At high crustal temperatures, the mineral sustains little radiation damage (Meldrum et al., 1998) and remains relatively impervious to Pb loss (Smith and Giletti, 1997) and thus is an excellent candidate for geochronology. Moreover, monazite inclusions in garnet may be further armored against daughter product loss because of the low solubility and permeability of Pb in the host (Montel, 1999; Montel et al., 2000). Geochronologic studies established that the MCT hanging wall was deforming in the Early Miocene (~22 Ma; Hodges et al., 1996), but in central Nepal, in situ Th–Pb monazite ages indicate the footwall was active at ~7 Ma, and as recently as ~3 Ma (Harrison et al., 1997a; Catlos et al., 1999, 2001). These results imply large-scale Late Miocene–Pliocene MCT reactivation (Harrison et al., 1997a, 1998), but it has not yet been shown that this event is common to the entire region.

In this paper we present in situ Th–Pb ion microprobe ages of monazite grains found as inclusions in garnet porphyroblasts and within the deformed rock matrix from

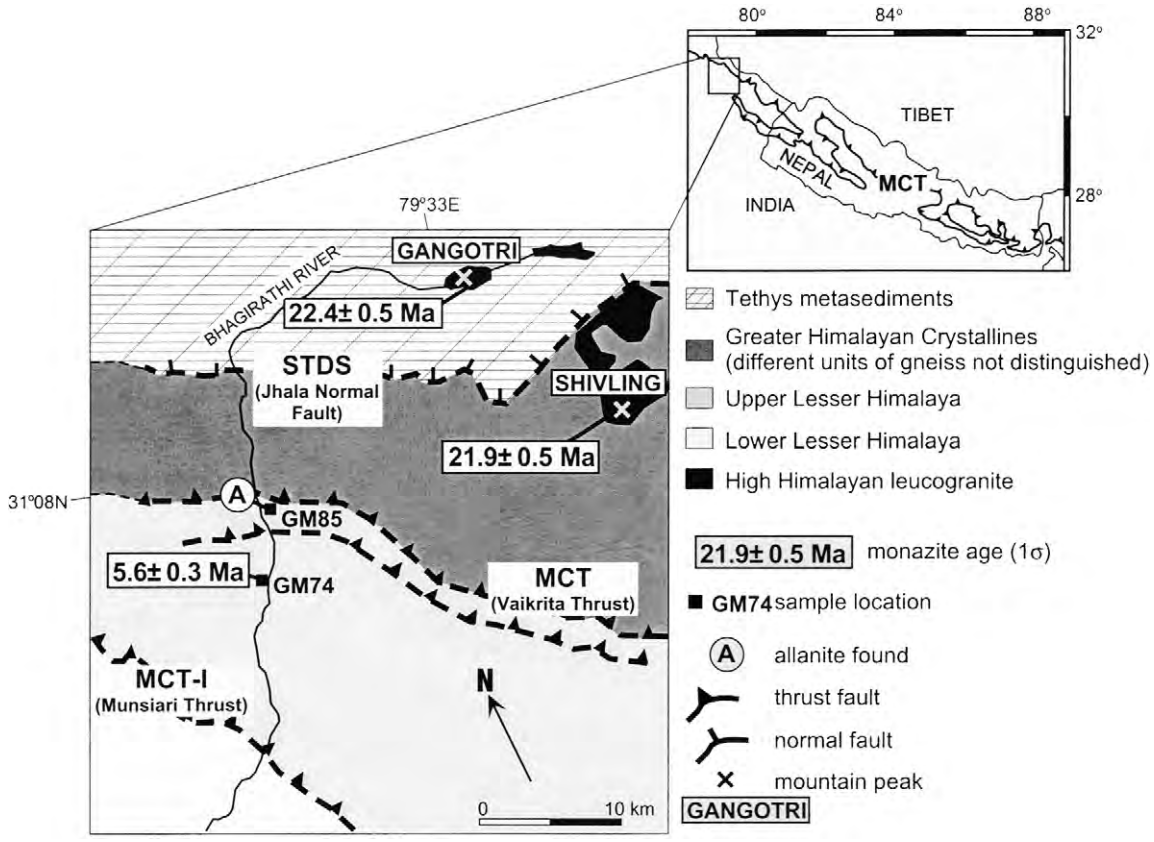

Fig. 2. Generalized geologic map of the Garhwal Himalaya, India after Metcalfe (1993) and Searle et al. (1999). Sample GM74 was collected within the upper Lesser Himalaya. Monazite ages for the Gangotri and Shivling leucogranites after Harrison et al. (1997b) and for sample GM74 is from this study. The upper right inset shows the location of the Garhwal area in context of country borders and the approximate lateral extent of the MCT. For further geologic information about the Garhwal Himalaya see Pêcher and Scaillet (1989), Metcalfe (1993), and Searle et al. (1999).

the Dudh Kosi-Everest region, eastern Nepal (Fig. 1) and from a locale ~800 km west, the Bhagirathi River, Garhwal Himalaya, India (Fig. 2). We combine these data with pressure–temperature (P–T) estimates from garnet-bearing metamorphic mineral assemblages. The technique reported here significantly differs from methods previously used (e.g., Hodges et al., 1996; Coleman, 1998; Simpson et al., 2000), in that these earlier efforts required mineral separation, eliminating textural relationships between the material being dated and those used to calculate the thermobarometric conditions. In situ analysis preserves the link between the P–T and timing information and reveals a protracted and complex metamorphic history of the units separated by the MCT.

2. Geologic overview

The Himalayan range is comprised of roughly parallel, large-scale fault systems that separate laterally continuous lithologies (see Upreti, 1999 for a review). Thus in eastern Nepal, structures and rocks are similar to those present in the Garhwal Himalaya (Figs. 1 and 2). The Dudh Kosi drainage has been intensely studied for ~40 yr (Lombard, 1952; Bordet, 1961; Amma and Akiba, 1967; Hagen, 1968; Kai, 1981; Kaneoka and Kono, 1981; Ferrara et al., 1983; Hubbard, 1989; Schelling, 1992; Pognante and Benna, 1993; Carosi et al., 1999a), whereas the Garhwal region was the focus of some of the earliest studies of Himalayan geology (e.g., Middlemiss, 1885;Middlemiss, 1887, 1888; Auden, 1937). Both study areas transect three fundamental Himalayan structures.

The Southern Tibetan Detachment System (STDS) separates low-grade Cambrian to mid-Eocene Tethys Formation rocks in its hanging wall from a Late Proterozoic unit of footwall gneisses called the Greater Himalayan Crystallines (Burg et al., 1984; Burchfiel et al., 1992). High Himalayan leucogranites intrude the lower Tethys Formation and upper structural levels of the Greater Himalayan Crystallines (Le Fort, 1975; Harrison et al., 1997b). The STDS in eastern Nepal consists of a lower ductile shear zone and an upper low-angle brittle fault, with the lower structure considered the principal extensional feature (Carosi et al., 1996, 1998, 1999a,b; Searle, 1999). The Jhala Normal Fault is considered the analogue to or part of the STDS in the Garhwal Himalaya (Pêcher and Scaillet, 1989; Metcalfe, 1993; Searle et al., 1993, 1999), and Miocene-age High Himalayan leucogranites are exposed on the peaks of

Gangotri and Shivling (Fig. 2) (Harrison et al., 1997b; Searle et al., 1999).

At its base, the Greater Himalayan Crystallines are thrust over Middle Proterozoic phyllites, metaquartzites, and mylonitic augen gneisses of the Lesser Himalaya Formation along the MCT (Brunel and Kienast, 1986; Schelling, 1992; Pognante and Benna, 1993). Lack of an obvious discontinuity between the Greater Himalayan Crystallines and Lesser Himalaya makes field identification of the fault problematic. An inverted metamorphic gradient characterizes the footwall (e.g., Hubbard, 1988). In eastern Nepal, two thrusts (MCT and MCT-I; e.g., Arita, 1983) bound a ductile MCT shear zone (i.e., upper Lesser Himalaya). Along the Dudh Kosi-Everest transect, the MCT corresponds to the contact between the Greater Himalayan Crystallines gneisses and the upper Lesser Himalayan pelitic schists, whereas the MCT-I separates the mylonitic Phaplu augen gneiss from low-grade Lesser Himalayan metasedimentary rocks. Along the Bhagirathi River, Garhwal region, the Vaikrita Thrust (i.e., MCT) and Munsiari Thrust (i.e., MCT-I) bound the MCT shear zone (Fig. 2), but no equivalent to the Phaplu augen gneiss is exposed (e.g., Valdiya, 1980; Metcalfe, 1993; Searle et al., 1993; Ahmad et al., 2000). As in eastern Nepal, no obvious break in metamorphic grade exists across the fault, and an inverted metamorphic sequence characterizes the footwall (Metcalfe, 1993; Ahmad et al., 2000).

Further south, other laterally continuous structures exist. The Main Boundary Thrust (MBT) separates the Lesser Himalaya from Neogene molasse, the Siwalik Formation (Seeber et al., 1981; Valdiya, 1992; Meigs et al., 1995). South of the MBT, the Main Frontal Thrust (MFT) typically defines the boundary between the Siwalik Formation and the northern Indo-Gangetic Plains (Yeats et al., 1992; Mugnier et al., 1999). The crustal-scale structures of the Himalayan range appear to sole into a common decollement termed the Main Himalayan Thrust (MHT) (Zhao et al., 1993; Nelson et al., 1996). At present, the Indian craton moves north-northeast at a rate of 44–61 mm yr^{-1} relative to Siberia (Minster and Jordan, 1978; Armijo et al., 1989; DeMets et al., 1990). Recent global positioning studies suggest this rate may be significant slower at 37–42 mm yr^{-1} (Chen et al., 2000; Shen et al., 2000).

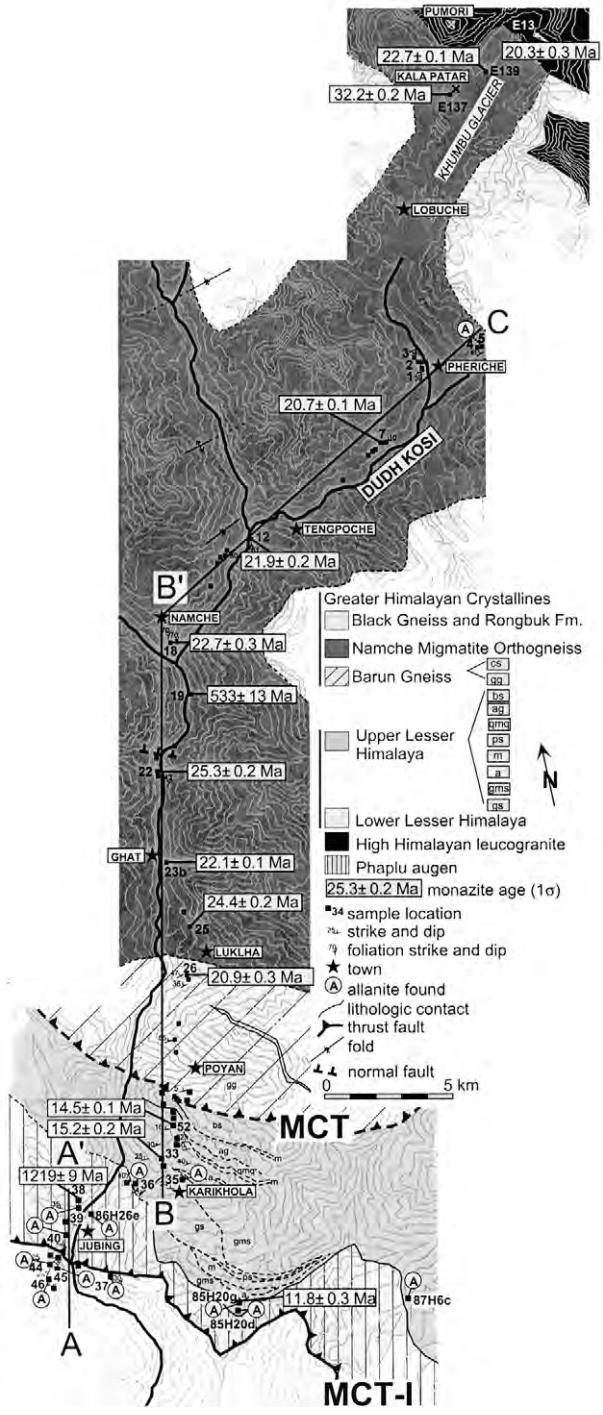

Fig. 3. Geologic traverse and sample location map along the Dudh Kosi, eastern Nepal. See Fig. 1 for the location of this area in context of the region. Contour interval is 200 m, based on the Dudh Kosi, Shorong Hinku, and Khumbu Himal 1:50000 topographic maps of Schneider et al. (1981a,b,c). All rocks sampled for this study are referred to as ET. Hubbard (1989) collected samples 86H26e, 85H20d, 85H20g, and 87H6c, whereas Simpson et al. (2000) collected samples E137, E139, and E13. The Greater Himalayan Crystallines include the Black Gneiss and Rongbuk Formation, Namche Migmatite Orthogneiss, and Barun Gneiss, cs, calc-silicate rock; gg, garnet-bearing gneiss. The upper Lesser Himalaya Formations include gs, graphitic schist; gms, garnet-mica schist; a, amphibolite; m, marble; ps, psammite; qmq, quartzite and micaceous quartzite; ag, augen gneiss; bs, biotite schist. Weighted mean Th–Pb monazite ages ($\pm 1\sigma$) from samples collected along this transect are in boxes. The age reported for ET26 is the average of the Miocene monazite grains only and the age reported for ET19 is the average of the Cambrian monazite grains only. Details of the ion microprobe results are available at http://oro.ess.ucla.edu/argonlab/data_repositiory.html, Tables 2 and 3. Town names are in boxes designated by stars, whereas mountain peak names are in boxes designated by crosses. The 'A' in the circle means that allanite is found in the sample and monazite was not found. All contacts are approximate when dashed and are based on Hubbard (1988), Lombardo et al. (1993), Simpson et al. (2000), and our field observations. See Fig. 4 for the geologic cross section along A–A′, B–B′, and B′ –C.

3. Previous work and suggested metamorphic histories

3.1. Dudh Kosi-Everest transect, eastern Nepal

Thermobarometric studies of samples of the Greater Himalayan Crystallines collected along the Dudh Kosi suggest the unit records three texturally and metamorphically distinct events (Pognante and Benna, 1993; Carosi et al., 1999b; Lombardo and Rolfo, 2000). First, the protolith, a thick sequence of clastic metasedimentary rocks intruded by granitoids, was subducted during the initial phase of collision (the Eocene-Oligocene Eohimalayan event, $T \approx 550$–680°C and $P \approx 8$–14 kbar). These rocks were then exhumed by two events during the Miocene. The first occurred at higher temperature and lower pressure ($T \approx 650$–800°C and $P \approx 4$–7 kbar), whereas the second was at lower pressure and temperature ($T \approx 500$–700°C, $P \approx 2$–4 kbar). During the second and third stages, the leucogranite magmas found in structurally higher levels of the MCT hanging wall form followed by the infiltration of metamorphic fluids (Pognante and Benna, 1993).

Thermobarometric analyses of garnet-bearing rocks collected along transects perpendicular to the MCT indicate that the Greater Himalayan Crystallines record pressures consistent with a lithostatic gradient (see Harrison et al., 1999a, Fig. 3). In eastern Nepal, pressures decrease from 7–8 kbar near the MCT to 2–4 kbar near the STDS (Brunel and Kienast, 1986; Hubbard, 1989). Temperatures tend to increase from the MCT zone and into the lower portion of the Greater Himalayan Crystallines (350–750°C; Pognante and Benna, 1993; Hubbard, 1989), and then trend lower from the middle to top (750–450°C; Pognante and Benna, 1993). Irregular temperature profiles within the unit may reflect unrecognized structural breaks, heating from granitic intrusions (Brunel and Kienast, 1986), or erroneous thermometric calculations (Kohn and Spear, 2001).

U–Pb ages of monazite grains separated from samples collected in higher structural levels of the Greater Himalayan Crystallines have been interpreted as evidence that ~20–25 my elapsed between the Eohimalayan event and subsequent exhumation and granite emplacement (e.g., Coleman, 1998; Walker et al., 1999; Simpson et al., 2000). In eastern Nepal, 17–21 Ma $^{40}Ar/^{39}Ar$ ages of Greater Himalayan Crystallines mica and hornblende have been linked to MCT slip and uplift of the range (Kaneoka and Kono, 1981; Hubbard and Harrison, 1989) and Early Miocene-age High Himalayan leucogranites are exposed (Schärer, 1984; Schärer et al., 1986). Apatite U–Th/He ages from samples collected from upper structural levels of the Greater Himalayan Crystallines and upper Lesser Himalaya along the Dudh Kosi-Everest transect are 6 ± 4 and 4.6 ± 0.2 Ma, but a sample near the town of Ghat yields a 0.8 ± 0.1 Ma age (Hubbard and House, 2000).

3.2. Garhwal Himalaya, India

Thermobarometric analyses of garnet-bearing rocks collected along the Bhagirathi River in the Garhwal Himalaya (Metcalfe, 1993; Manickavasagam et al., 1999) indicate that temperatures increase from 500 to 770°C across the MCT zone, and then decrease within the Greater Himalayan Crystallines to 550–640°C. Pressures increase from 6 kbar within the MCT zone to 10–12 kbar at the base of the Greater Himalayan Crystallines, and then level off within the unit at 7–9 kbar. High Himalayan leucogranites in this area yield Th–Pb monazite ages of 22.4 ± 0.5 Ma (Gangotri), 21.9 ± 0.5 Ma (Shivling; Harrison et al., 1997b), 23.0 ± 0.2 Ma (Shivling U–Pb age, Searle et al., 1999), whereas 17–22 Ma $^{40}Ar/^{39}Ar$ mica ages are found in upper Lesser Himalaya and Greater Himalayan Crystallines rocks (Metcalfe, 1993). Foster et al. (2000) found monazite inclusions in garnet grains from two rocks from the Greater Himalayan Crystallines collected adjacent to the Bhagirathi River that range in age from 43.4 ± 2.5 to 36.3 ± 2.0 Ma (Th–Pb age, $\pm 2\sigma$). Matrix grains are within error or younger than the monazite inclusions (40–26 Ma) and Foster et al. (2000) support the interpretation that the younger ages represent crystallization. Alternatively, matrix grains may have experienced diffusional reequilibration after the garnet inclusions closed to Pb loss.

From P–T data and mica ages, Metcalfe (1993) suggests a polyphase metamorphic evolution for the Bhagirathi River region. First, Barrovian metamorphism and anatectic melts developed within the Greater Himalayan Crystallines (i.e. Eohimalayan metamorphism), followed by Miocene slip along the MCT and activation of the Jhala Normal Fault. Subsequent rapid erosion is invoked to preserve the metamorphic assemblages observed in the field today. Slip along the Jhala Normal Fault is suggested to form folds in the Tethys Formation and further develop and generate anatectic melts now exposed on the peaks of Shivling and Gangotri.

3.3. Models for the evolution of the Himalaya

The geochronologic and thermobarometric studies of rocks collected along the Dudh Kosi-Everest transect and Garhwal Himalaya led to the proposal that the Greater Himalayan Crystallines extruded as a coherent wedge due to large-scale thrusting along the MCT occurring simultaneously with extension along the STDS (e.g., Hodges et al., 1992; Metcalfe, 1993; Pognante and Benna, 1993; Carosi et al., 1999b; Grujic et al., 1999; Lombardo and Rolfo, 2000). Geophysical data are consistent with the faults that bound the Greater Himalaya Crystallines converging at depth (Nelson et al., 1996), leaving open the wedge-extrusion possibility and suggesting that compressional and gravitational forces compete for control of the orogenic profile.

Another hypothesis emphasizes the influence of

transposition of right-way-up metamorphic sequences during Late Miocene and Pliocene slip within the MCT shear zone (Harrison et al., 1998). A footwall rock from central Nepal contains matrix monazite grains that crystallized at ~3 Ma, requiring the MCT to accommodate a substantial fraction of shortening between India and Asia (Catlos et al., 1999, 2001). However, the lateral extent of this reactivation event is incompletely known and obtaining additional geochronologic analyses of monazite grains from rocks at similar structural levels along the range front is the primary means to evaluate this hypothesis.

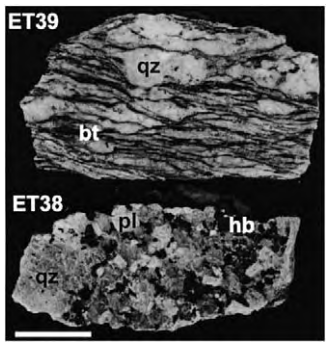

Fig. 5. Two samples ET39 (upper) and ET38 (lower) from the Phaplu augen gneiss unit collected south of the town of Jubing (see Fig. 3). ET39 is a typical example the Phaplu augen gneiss and ET38 was collected near the ET39 outcrop; qz, quartz, pl, plagioclase, bt, biotite, hb, hornblende. In ET38, garnet appears as small inclusions in hornblende. Th–Pb ion microprobe analyses of monazite grains from ET38 yield 1.6–0.9 Ga ages. The scale bar is ~15 mm.

4. Sample selection and petrography

4.1. Dudh Kosi-Everest transect, eastern Nepal

Samples were collected south of Mt. Everest in a ~45 km transect along the Dudh Kosi drainage (Figs. 1, 3, and 4), extending ~1 km south of the MCT shear zone to the base of the Khumbu icefall within the Greater Himalayan Crystallines. Detailed petrologic descriptions of rocks collected along the Dudh Kosi have been previously reported (Hubbard, 1988, 1989; Pognante and Benna, 1993).

The lower Lesser Himalaya (Okhaldhuga Unit) consists of a low-grade green phyllite with the mineral assemblage chlorite + plagioclase + muscovite + rutile + tourmaline + epidote (allanite) + quartz ± garnet. Garnets in this formation are only found near the contact with the overlying augen gneiss, and are small (~1–2 mm), euhedral, and in close association with chlorite. Pods of quartz and plagioclase are sometimes found in these rocks.

Above the lower Lesser Himalaya, the Phaplu augen gneiss appears as a ~4 km thick package. Fig. 5 shows two rock samples, ET38 and ET39, collected south of the town of Jubing. ET39 is a typical example of the augen gneiss, a blue-grey rock that contains rounded quartz + K-feldspar + plagioclase + biotite + muscovite + chlorite + sphene + rutile + sillimanite + allanite. Sample ET38 was collected near the ET39 outcrop and the undeformed texture suggests that ET38 may represent the protolith of the Phaplu augen gneiss. However, the mineral assemblages indicate the rocks are of different composition. ET38 is comprised of small, euhedral garnets (<0.5 mm-sized) encompassed in larger grains of hornblende + quartz + plagioclase + biotite + chlorite + muscovite + rutile. ET38 also contains ~500 μm-sized grains of matrix monazite and zircon.

Above the Phaplu augen gneiss, the upper Lesser Himalaya appears as a ~5 km thick sequence of quartzite, graphitic and garnet-bearing schists, and augen gneiss. Monazite is found within the upper Lesser Himalaya in pelitic bulk compositions south of the sillimanite isograd. The garnet-bearing assemblages of the upper Lesser Himalaya contain garnet + sillimanite + biotite + muscovite + albite + tourmaline + ilmenite + monazite ± allanite + quartz. Pognante and Benna (1993) observed kyanite in a single sample along this transect, but it is absent in the rocks we collected. Small mats of fibrous sillimanite appeared in the rock matrix, whereas biotite and plagioclase are typical inclusions in garnet. Sample 85H20g, collected ~5 km east of the Dudh Kosi drainage, has a similar upper Lesser Himalayan assemblage, but contains staurolite and no sillimanite. Garnet-biotite thermometry indicates this garnet experienced a maximum temperature of 530 ± 50°C (see Hubbard, 1989).

Lombardo and Rolfo (2000) report a complicated MCT zone with three sheets sandwiched between the base of the Greater Himalayan Crystallines and the lower Lesser Himalaya. The presence and location of these structures

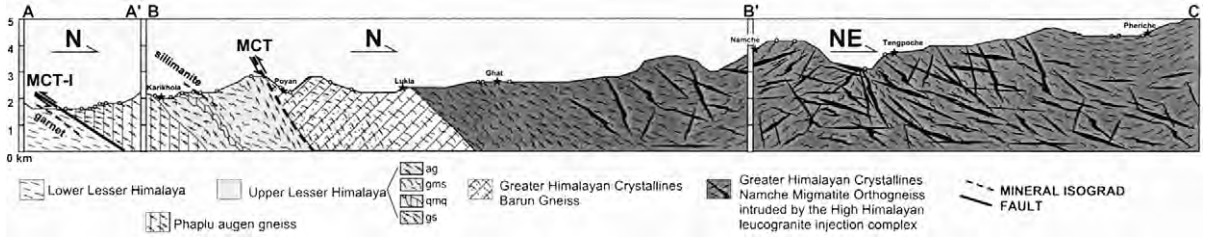

Fig. 4. Geologic cross section along the Dudh Kosi in eastern Nepal. For lines of section, see Fig. 3. A star indicates a town. Faults are designated by darker lines, whereas mineral isograd lines are dashed. All contacts are approximate when dashed. The upper Lesser Himalaya Formations include ag, augen gneiss; gms, garnet-mica schist; qmq, quartzite and micaceous quartzite; gs, graphitic schist.

are inconsistent with our observations (Fig. 3). There is no break in mineral assemblage or structure across the MCT, located near the town of Poyan (see also Hubbard, 1988). The break is based on the appearance of Greater Himalayan Crystallines migmatites and an apparent decrease in strain (Hubbard, 1988; Lombardo et al., 1993).

The Greater Himalayan Crystallines are separated here into different gneiss units (e.g., Pognante and Benna, 1993; Carosi et al., 1999a). The base, called the Barun Gneiss, is a complex of migmatized paragneiss with minor metabasites, calc-silicate rocks and marbles. The middle unit, the Namche Migmatite Orthogneiss, is thought to be a pre-Himalayan granitoid that intruded a sequence of metasedimentary rocks and was subsequently metamorphosed. The contact between the Barun Gneiss and Namche Migmatite Orthogneiss is unclear in the field because both units have a similar lithology: biotite + muscovite + albite + sillimanite + quartz ± garnet ± tourmaline + ilmenite + zircon ± monazite. The location of the contact in Fig. 3 is based on Lombardo et al. (1993). The upper paragneiss unit, called the Black Gneiss, may have been the sedimentary cover of the Namche Migmatite Orthogneiss (Pognante and Benna, 1993). Along the Dudh Kosi-Everest transect, folds appear within upper structural levels of the Greater Himalayan Crystallines (Figs. 3 and 4), and their origin has been linked to extension along the STDS (e.g., Carosi et al., 1999b).

Tourmaline leucogranites intrude the Namche Migmatite Orthogneiss and both crosscut the main fabric and appear ductily deformed. The leucogranites have the mineral assemblage: quartz + albite + biotite + sillimanite + tourmaline ± apatite + monazite + zircon. The injection complex increases in outcrop abundance from the town of Ghat to Tengpoche, but near Pheriche little leucogranite appears (Fig. 4). Rocks collected near Pheriche (samples ET1–ET5) contain green biotite + tourmaline + plagioclase + muscovite + sillimanite + apatite + rutile + quartz ± garnet ± allanite.

4.2. Garhwal Himalaya, India

Samples GM74 and GM85 were collected by Metcalfe (1993) beneath the MCT along the Bhagirathi River, Garhwal Himalaya, India (see Fig. 2). GM85 has the mineral assemblage garnet + biotite + chlorite + muscovite + plagioclase + tourmaline + rutile + allanite + quartz, whereas GM74 has a similar assemblage, but contains monazite, and no allanite or garnet. Although we lack pressure and temperature constraints for these specific samples, a rock collected near GM74 yields 500 ± 40°C and 7 ± 2 kbar (sample GM72). Note that the temperature is well below the closure temperature for Pb in monazite (Smith and Giletti, 1997). For further geologic information about the Garhwal Himalaya see Pêcher and Scaillet (1989), Metcalfe (1993), and Searle et al. (1999).

5. Methods for geochronologic and thermobarometric analyses

Several thermobarometric estimates have been previously calculated for the garnet-bearing assemblages collected along the Dudh Kosi-Everest transect and the Garhwal Himalaya (Hubbard, 1989; Pognante and Benna, 1993; Metcalfe, 1993), but the P–T conditions reported for these transects may be affected by substantial errors (Kohn and Spear, 2001). In this paper, X-ray compositional maps of garnet were only obtained for samples ET19, ET52, ET33, and ET45. The maps were used to qualitatively evaluate garnet zoning patterns in Mn, Ca, Fe, and Mg, and assure that the areas chosen for quantitative analysis represent the lowest Mn and Fe/(Fe + Mg) values and therefore attempt an estimate of the minimum peak P–T conditions recorded by the garnet (e.g., Spear and Peacock, 1989). All thermobarometric information is available as a supplement at http://oro.ess.ucla.edu/argonlab/data_repositiory.html.

Compositions of garnet, muscovite, plagioclase, biotite, and chlorite were obtained with a JEOL electron microprobe operating at an accelerating potential of 20 kV and a primary current of ~10 nA. Maximum count-times were 20 s, and all raw data were reduced using the ZAF matrix correction. The garnet–biotite thermometer of Ferry and Spear (1978) with the Berman (1990) garnet solution model and the garnet–plagioclase–biotite–muscovite barometer of Hoisch (1990) were used. Biotite was not found in sample ET45, so the garnet–chlorite thermometer of Dickenson and Hewitt (1986) and Laird (1988) along with the Berman (1990) garnet solution model was used.

Monazite grains were located in several rock thin sections using backscattered electron petrography. Sample ET7, the structurally highest sample analyzed in this study, is a tourmaline-bearing High Himalayan leucogranite, observed in the field as part of an extensive injection complex (Fig. 4). The other samples are garnet-bearing assemblages of the Greater Himalayan Crystallines Namche Migmatite Orthogneiss (ET12, ET18b, ET19, ET22, ET23b, ET25), Barun Gneiss (ET26), upper Lesser Himalaya (ET52, ET33, 85H20g, GM74), and Phaplu augen gneiss (ET38).

Monazite grains in these rocks are irregularly shaped, zoned, and vary in size from 15 to 500 μm. The portion of the thin section containing the minerals used for thermobarometry and geochronology was trimmed and mounted in epoxy with monazite age standards (Harrison et al., 1999b). The 1 in. diameter mount was then gold coated and the monazite grains analyzed with a CAMECA ims 1270 ion microprobe using methods described by Harrison et al. (1995). Because the grains were typically about the size of the oxygen beam (20–30 μm in diameter) and owing to the difficulty of locating the monazites in polished rock thin section using the optical systematics of the ion microprobe, we did not attempt to link the ages to compositional zoning. The uncertainty in the Th–Pb ages reported in this paper is

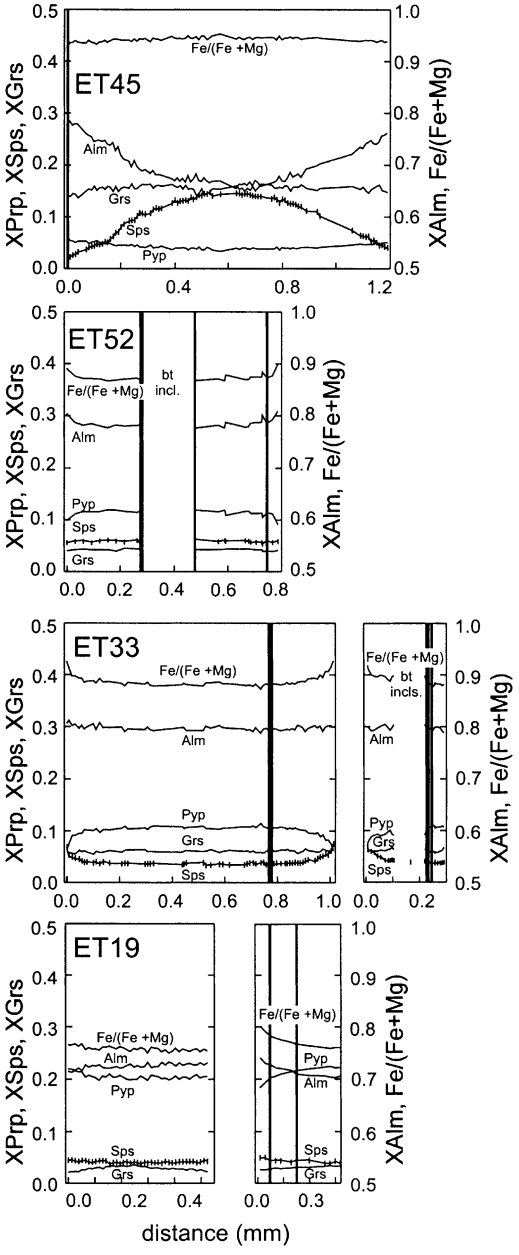

Fig. 6. Zoning profiles of mole fraction spessartine (Sps), grossular (Grs), almandine (Alm), pyrope (Pyp), and Fe/(Fe + Mg) across ET45, ET52, ET33, and ET19 garnets. All traverses were made from rim to rim along the garnet, and ET19 and ET33 include a traverse (right) that extends from mid-core (~0.3–0.4 mm) to rim (0.0 mm). Distance scale in each is identical. See Fig. 7 for the position of the compositional traverse along ET33 and ET52. Tick marks on the spessartine profiles show the position of each analysis; the length of each tick has no statistical significance. The bold vertical lines are positions of compositions used for *P–T* calculations; see Table 1 for numerical values.

limited by the reproduction of a calibration curve, and is approximately ±2%. All ion microprobe monazite ages are quoted at the level of 1σ. Details of the geochronologic analyses and backscattered electron images of the grains dated in this study are available at http://oro.ess.ucla.edu/argonlab/data_repositiory.html.

6. Thermobarometric results

6.1. Garnet zoning

Compositional traverses across garnets from the lower Lesser Himalaya are strikingly different from those collected from the upper Lesser Himalaya and Greater Himalayan Crystallines (Fig. 6). Sample ET45, collected <1 km beneath the MCT-I (Fig. 3), is an example of a lower Lesser Himalayan garnet. The garnet has a dome-shaped profile in spessartine, with a maximum mole fraction of ~0.145 in the core, and minimum of ~0.04 at the rim, consistent with prograde growth (e.g., Spear, 1993). The Fe/(Fe + Mg) content of the garnet is flat, but slight decreases near the rim suggest it grew with increasing temperature (e.g., Spear et al., 1990).

The zoning pattern of ET45 stands in stark contrast to those seen in samples from the upper Lesser Himalayan (ET52 and ET33) or Greater Himalayan Crystallines sample (ET19; see Fig. 6). The high-grade garnets contain mole fraction spessartine of ~0.04 within the cores that increase only at the rim (to ~0.05 for ET19 and ~0.08 for ET33), consistent with diffusion or significant back-reaction involving garnet retrogression (e.g., Spear, 1993). Grossular compositions in all the garnets analyzed are relatively flat, although ET19 decreases slightly from core to rim, indicating the garnet may contain a remnant record of exhumation. The profiles reported here are similar to Greater Himalayan Crystallines garnets from NW India, central Nepal, and Bhutan (e.g., Hodges et al., 1993; Metcalfe, 1993; Kaneko, 1995; Davidson et al., 1997; Vannay and Grasemann, 1998).

6.2. Pressure and temperature calculations

Table 1 lists the mineral compositions and P-T results from samples ET52, ET19, ET33 and ET45, which were collected along the Dudh Kosi-Everest transect. To estimate the minimum peak temperature recorded by the ET45 garnet, the minimum Mn garnet composition, equivalent to the lowest Fe/(Fe + Mg), with matrix chlorite yields a temperature of 550 ± 20°C (at $P \approx 3$–8 kbar, see Table 1 and Fig. 6). Unfortunately, monazite is absent in sample ET45 and is not found in samples collected near this rock (Fig. 3). Allanite appears as the only rare-earth bearing accessory mineral, and attempts to date grains using the Th–Pb ion microprobe methods outlined in Catlos et al. (2000) were unsuccessful due to high common Pb concentrations.

As an initial step in deciphering the thermobarometric conditions recorded by the Greater Himalaya Crystallines samples, garnet compositions with minimum Mn and Fe/(Fe + Mg) were combined with matrix biotite, muscovite, and plagioclase compositions (Table 1; Fig. 6). Sample ET33 yields 720 ± 40°C and 10 ± 1 kbar, whereas sample ET19, collected at higher structural levels, records a similar pressure to ET33 but higher

Table 1
Compositional parameters used in the geothermobarometric calculations

Sample[a]	Biotite[b]		Garnet[c]			Plag[d]	P (kbar)[e]	T (°C)[f]
	XFe	XMg	XMn	XCa	FM	XAn		
ET52								
(Rim + Matrix)	0.614	0.385	0.057	0.039	0.876	0.189	7.2	690
	0.605	0.392	0.057	0.039	0.876	0.200	6.6	673
(Core + Inclusions)	0.553	0.445	0.062	0.042	0.880	0.201	5.4	581
	0.547	0.450	0.062	0.042	0.880	0.216	4.9	571
	0.553	0.445	0.061	0.044	0.872	0.201	6.0	606
	0.547	0.450	0.061	0.044	0.872	0.216	5.5	595
	0.553	0.445	0.056	0.044	0.869	0.201	6.2	617
	0.547	0.450	0.056	0.044	0.869	0.216	5.7	606
ET19								
(Rim + Matrix)	0.484	0.515	0.040	0.030	0.770	0.155	9.3	778
	0.499	0.497	0.038	0.034	0.758	0.137	11.1	882
ET33								
(Rim + Matrix)	0.619	0.379	0.036	0.059	0.883	0.190	8.7	693
	0.641	0.357	0.037	0.063	0.882	0.189	10.3	749
(Core + Inclusions)	0.569	0.428	0.037	0.060	0.882	0.242	7.0	617
	0.572	0.426	0.037	0.060	0.882	0.201	7.3	619
	0.572	0.426	0.039	0.057	0.882	0.242	6.2	614
	0.578	0.419	0.039	0.057	0.882	0.201	7.3	628
	0.578	0.419	0.040	0.061	0.886	0.242	6.4	612
	0.586	0.412	0.040	0.061	0.886	0.201	7.4	626
Sample	Chlorite[g]		Garnet					T (°C)[h]
	XFe	XMg	XMn	XCa	FM			
ET45								
(Rim + Matrix)	0.626	0.372	0.041	0.147	0.938	–	–	550 ± 20
	0.634	0.363	0.041	0.147	0.938	–	–	–

[a] Sample name and location of compositional analyses; (rim + matrix), analyses taken from the garnet rim and matrix grains; (core + inclusions), analyses of the garnet core and inclusions. See Fig. 3 for sample locations and Fig. 6 for garnet zoning profiles and locations of the garnet compositions.
[b] Biotite mole fraction, XFe = Fe/(Fe + Mn + Mg) and XMg = Mg/(Fe + Mn + Mg).
[c] Garnet mole fraction XMn = Mn/(Ca + Fe + Mn + Mg); XCa = Ca/(Ca + Fe + Mn + Mg); and FMFe/(Fe + Mg).
[d] Plagioclase anorthite mole fraction, XAn = Ca/(Na + K + Ca).
[e] Pressure calculated using the mineral compositions listed and the garnet–plagioclase–biotite–muscovite barometer of Hoisch (1990).
[f] Temperature calculated using the mineral compositions listed and the garnet-biotite thermometer of Ferry and Spear (1978) with the Berman (1990) garnet solution model.
[g] For ET45, the compositions listed are for matrix chlorite grains (instead of biotite), and plagioclase compositions were not taken.
[h] The garnet–chlorite temperature between 3 and 8 kbar using the mineral compositions listed and the thermometer of Dickenson and Hewitt (1986) and Laird (1988) with the Berman (1990) garnet solution model.

temperature conditions of 830 ± 75°C. The abundance of muscovite and the absence of partial melting textures in sample ET19 are inconsistent with the P–T results. Retrograde net transfer reactions that cause mineral growth and dissolution within high-grade rocks may have significantly affected the ET19 garnet and resulted in a higher temperature than the actual peak (Spear, 1991; Kohn and Spear, 2001).

Garnets from samples ET33 and ET52 contain biotite inclusions (Fig. 7), suggesting that core temperatures can be estimated using the flat garnet core composition and inclusions. To discern the P–T path followed by ET33, core pressure were calculated using the compositions of plagioclase and biotite inclusions (e.g., St-Onge, 1987). For ET52, plagioclase inclusions are not found within the garnet, but matrix plagioclase is zoned (Table 1). For this rock, core pressure was calculated using the matrix plagioclase core composition along with the biotite inclusions.

Thermobarometric calculations using garnets that appear affected by diffusion can create misleading results (e.g., Florence and Spear, 1991), but the ET52 biotite inclusion is rimmed by quartz in the two-dimensional thin section view, so we assume diffusional exchange of Fe and Mg did not significantly alter the biotite composition. This assumption may be invalid, because the biotite inclusion compositions for both samples ET52 and ET33 are more Mg rich than those within the matrix, indicating the temperature reported here may be erroneous and lower than actually experienced by the rock (e.g., Spear and Peacock, 1989). In addition, detailed compositional traverses along the garnet for ET33 show the garnet increases in Fe/(Fe + Mg) from 0.880 to 0.898 nearing the biotite (Fig. 6). To estimate core temperatures, the lowest

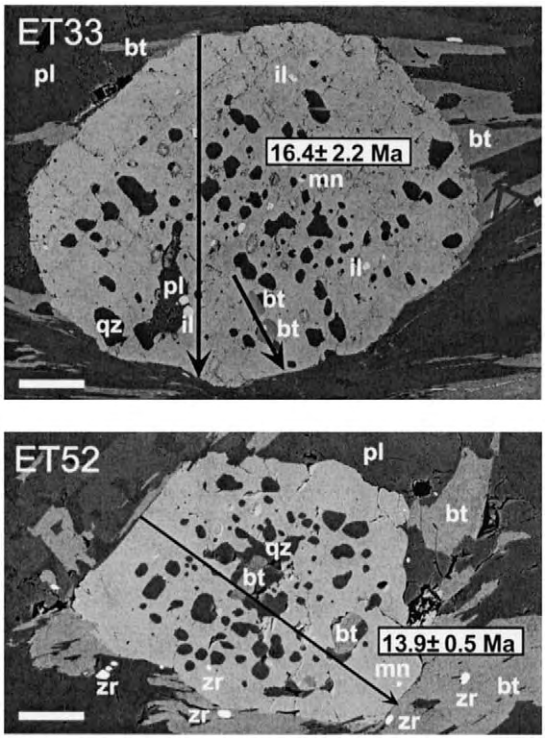

Fig. 7. Backscattered electron images of upper Lesser Himalaya garnets ET33 (upper) and ET52 (lower); pl, plagioclase; bt, biotite; il, ilmenite; qz, quartz; zr, zircon; mn, monazite inclusion in garnet with Th-Pb ion microprobe age (1σ) indicated. Arrows indicate locations of the compositional traverses in Fig. 6. See Fig. 8 for P–T paths calculated for these samples. The scale bar is 200 μm.

garnet Fe/(Fe + Mg) nearest to the biotite inclusion was taken along with the highest Fe/(Fe + Mg) biotite inclusion compositions (Table 1; Fig. 6).

Fig. 8 displays the P–T paths followed by samples ET52 and ET33. These rocks were collected ~2 km apart within the upper Lesser Himalaya (Fig. 3) and follow similar directions within P–T space indicating garnet growth with

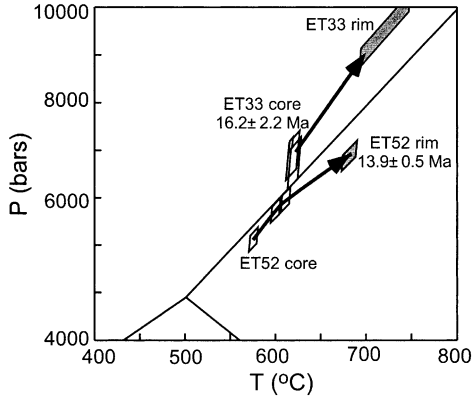

Fig. 8. P–T paths calculated for samples ET33 and ET52. See Fig. 3 for sample locations and Fig. 6, Table 2, and the data repository for compositional information used to obtain these values. Hollow boxes indicate P–T data calculated using garnet core compositions, whereas garnet rim conditions are shaded. Th–Pb ages for monazite inclusions in the core of the ET33 garnet and the rim of the ET52 garnet are indicated with 1σ error.

increasing pressure and temperature. The estimates fall within the sillimanite field for ET52, but not for ET33, consistent with our observations of the mineral assemblages and those by Pognante and Benna (1993).

7. Geochronologic results

Figs. 2 and 3 and Tables 2 and 3 summarize geochronologic data. The ages reveal a protracted and complex metamorphic history of these lithologies, which extend from the Paleo-Mesoproterozoic to the Late Miocene. Attempts to link the geochronologic data to deformation events affecting these samples are described below. All Th–Pb ion microprobe monazite ages are quoted at the level of 1σ.

7.1. Paleo-Mesoproterozoic (2500–900 Ma): the assembly of the Indian subcontinent

The Indian subcontinent is a complex of tectonic and stratigraphic terranes, which were juxtaposed along sutures during different periods of the Earth's history (e.g., Radhakrishana, 1989). In the Precambrian, components of the continent existed as the northern Bundelkhand Block, the southern South Indian Block, and the eastern Trans-Aravalli Block (Balasubramaniyam et al., 1978; Mazumder et al., 2000). Contrasting paleomagnetic and other geologic signatures from these blocks indicate they each record an isolated, unrelated evolution on different lithospheric plates during the Proterozoic (Qureshy and Iqbaluddin, 1992). For example, paleomagnetic data from the Cuddapah basin in the South Indian Block and the Vindhyan Basin in the Bundelkhand Block suggest these coeval basins evolved in the southern and northern hemispheres, respectively (Reddy and Prasad, 1979).

The South Indian Block and the Bundelkhand Block collided ~900 Ma along the Satpura Suture Zone (SSZ; a.k.a the Narmada-Son lineament), a prominent tectonic feature of the Indian Shield trending from the west coast of India to the eastern side (Mishra, 1992; Qureshy and Iqbaluddin, 1992; Rao, 1992). Today, the SSZ is active, characterized by heat flow and present-day seismicity comparable to that of the convergent Himalayan boundary (Bhatia et al., 1999).

The oldest ages reported for monazite in this study are matrix grains analyzed in a rock collected within the Phaplu augen gneiss (sample ET38; Fig. 5). This augen gneiss unit outcrops in central Nepal as well (Colchen et al., 1980). Spots on monazite grains in ET38 yield ages of 901 ± 13 to 1566 ± 49 Ma, whereas zircon ages from an equivalent augen gneiss are ~1831 Ma (DeCelles et al., 2000). A Lesser Himalayan monazite grain from central Nepal is ~1640 Ma (Catlos et al., 2001). Paleoproterozoic whole-rock Rb–Sr ages are also reported for Lesser Himalayan rocks from the Garhwal region (1907 ± 91 Ma; Ahmad et

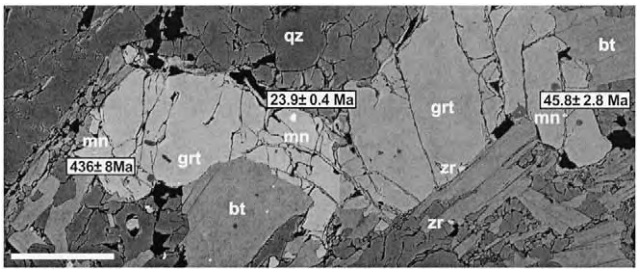

Fig. 9. Backscattered electron image of Greater Himalayan Crystallines sample ET26; mn, monazite inclusion in garnet; grt, garnet. Th–Pb ages are in boxes with 1σ errors. The scale bar is 300 μm. See Fig. 3 for sample location.

al., 1999). These ages reflect tectonic or magmatic events related to or older than the assembly of India.

7.2. Cambro-Ordovician (440–544 Ma): the suturing of India to Gondwana

Another episode that influenced the tectonic design and sedimentation history of the Himalaya was the Pan-African event, which has been well-described in Africa and western Europe (Duppert et al., 1990; Rabi et al., 1990). The Indian Pan-African event is characterized by an abrupt cessation of a long, almost unbroken cycle of Proterozoic sedimentation towards the close of the Lower Cambrian (Fuchs, 1968; Garzanti et al., 1986), and extensive emplacement of ~500 Ma granite bodies (Le Fort et al., 1986).

Gondwana sediments are present in two domains within the Himalaya: the Lesser Himalaya and the Tethys Formation (Tripathi and Singh, 1987). During the Cambrian, the Lesser Himalaya and Peninsular India were characterized by a wholesale suspension of sedimentation, whereas the Tethys Formation experienced an interruption in basin-filling (Valdiya, 1993). The sedimentary evidence suggests the presence of the Pan-African orogenic event in the northwestern Himalaya during which time the Indian shield gradually rose from the ocean. The Lesser Himalaya emerged towards the close of the Lower Cambrian, whereas the Tethys marginal basin surfaced in the Late Upper Permian (Valdiya, 1995). Due to the gap in deposition, the position of Gondwana during the Cambrian to Triassic is uncertain (e.g., Smith, 1999).

Cambro-Ordovician granite bodies are present throughout the Himalayan realm (Le Fort et al., 1986; Valdiya, 1993), and monazite grains of this age range reside in rocks of the Greater Himalayan Crystallines. For example, a 548 ± 17 Ma monazite inclusion in garnet is found in Namche Migmatite Orthogneiss sample ET19, whereas a monazite inclusion from Barun Gneiss sample ET26 yields 436 ± 8 Ma (Fig. 9). The inclusion in ET26 is young for the Pan African orogenic episode (e.g., Le Fort et al., 1986), but this sample has been through at least three monazite growth events and the age may time closure temperature (as opposed to crystallization), Pb loss via partial dissolution, or diffusion prior to occlusion by the garnet. Similarly, the 141–246 Ma matrix monazite grains within ET19 may reflect a 500 Ma grain that lost Pb, or overlapping analyses on grains that experienced subsequent growth or dissolution. These grains may serve as source materials for monazite precipitation during subsequent metamorphism.

Cambro-Ordovician mineral ages appear within the Greater Himalayan Crystallines elsewhere in the range. For example, in the Himachal Himalaya, Rb-Sr whole rock ages are 545 ± 12 and 311 ± 6 Ma (see Bhargava and Bassi, 1994). Sm–Nd isotopic analyses on garnets and whole rocks from the Garhwal region yield 534 ± 24 Ma (Argles et al., 1999) and monazite grains collected in the northwest Himalaya have an average U–Pb age of 467 ± 3 Ma (Foster, 2000). An allanite inclusion in garnet from the MCT shear zone in central Nepal gave a Th–Pb age of 445 ± 16 Ma (Catlos et al., 2000).

7.3. Eocene–Oligocene (54–23 Ma): from Indo-Asia collision to the Eohimalayan event

During the Cretaceous to the Eocene, India separated from Gondwana and drifted ~4000 km northward at rates of 15–20 cm yr^{-1} (Klootwijk et al., 1985; Royer and Sandwell, 1989). Paleomagnetic and stratigraphic data indicate that suturing between India and Asia completed by 55–45 Ma (e.g., Patzelt et al., 1996; Rowley, 1996, 1998). Analysis of the Zhepure Mountain stratigraphic section north of Mt. Everest is consistent with collision initiating no older than 47 Ma and probably younger than 45 Ma (Rowley, 1998). A monazite inclusion in garnet from Greater Himalayan Crystallines sample ET26 gives an age of 45.8 ± 2.8 Ma (Fig. 9), whereas a matrix grain yields a more precise age of 44.5 ± 0.9 Ma. The geochronologic data suggests that in eastern Nepal, the Greater Himalayan Crystallines were rapidly metamorphosed to temperatures that allowed monazite crystallization during the deposition of Zhepure Mountain sequence.

Remnants of the metamorphic history of the Greater Himalayan Crystallines since the Eocene are reported as Oligocene garnet ages (33–28 Ma, Vance and Harris, 1999; 44–36 Ma, Foster, 2000; Foster et al., 2000), and U–Pb ages of monazite grains (33–29 Ma, Walker et al., 1999; 36–25 Ma, Foster, 2000; ~32 Ma, Simpson et al., 2000). In sample ET18b, matrix monazite ages are 39.5 ± 0.8 and 33.5 ± 1.2 Ma. These ages may record the Eohimalayan event, in which the protolith of the Greater Himalayan Crystallines was buried beneath the southern edge of Asia (e.g., Le Fort, 1996).

Monazite inclusions in garnet with ages close to the Oligocene–Miocene boundary (~23 Ma) are also found in several rocks of the Greater Himalayan Crystallines. For example, sample ET22 (Fig. 10) contains monazite inclusions that are 19.4 ± 0.5 to 28.1 ± 0.5 Ma. The textural relationship between monazite and allanite coexisting the crack of the ET22 garnet (Fig. 10) implies that allanite

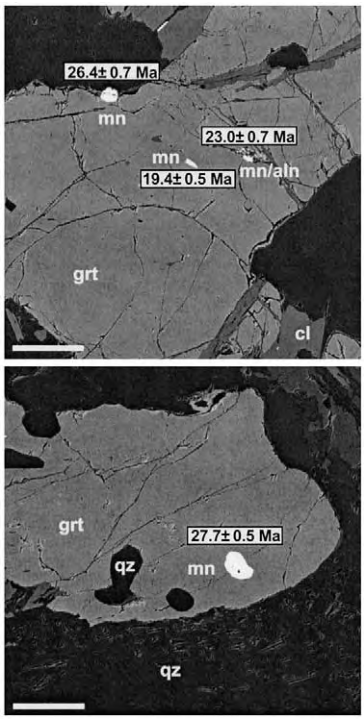

Fig. 10. Backscattered electron image of Greater Himalayan Crystallines sample ET22; mn, monazite inclusion in garnet; mn/aln, monazite exists in close reaction with allanite along a crack in the garnet; grt, garnet; cl, chlorite; qz, quartz. Th-Pb monazite ages are indicated with 1σ error. The age reported for the monazite grain in the lower image corresponds to the average of data from three ion microprobe spots. The scale bar is 200 μm. See Fig. 3 for sample location.

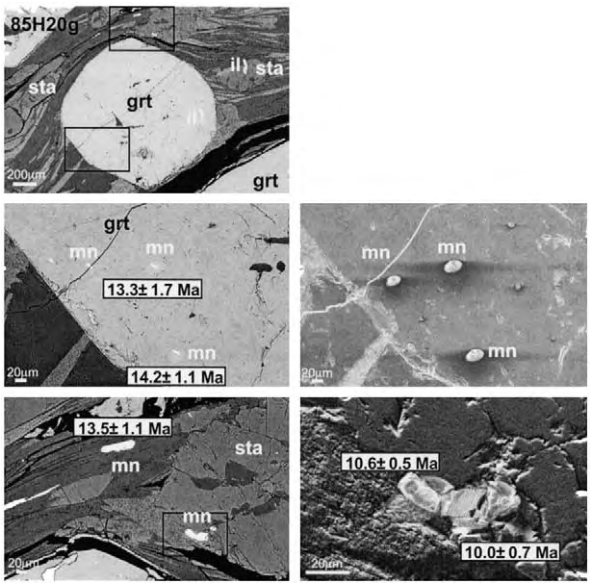

Fig. 11. (Left) Backscattered electron images and (right) secondary electron images of upper Lesser Himalaya sample 85H20g; grt, garnet; mn, monazite; sta, staurolite; il, ilmenite. See Fig. 3 for sample location. Th–Pb monazite ages are indicated with 1σ error. Boxes on the upper image show the approximate locations of the lower images. The oval spots in the secondary electron images are craters created by the ion microprobe beam. Secondary electron images are included in this figure to emphasize the difficulty in locating the monazite grain in polished rock thin section and to illustrate that most grains were typically about the size of the ion microprobe beam. Note that the beam was not placed on one monazite in the upper-right image because the grain could not be located, whereas two grains are wholly enveloped and two spots are placed on another grain in the lower-left image.

may be replacing monazite during alteration (e.g., Finger et al., 1998) as evidenced by the close proximity of the grains to the chlorite vein in the garnet. The presence of monazite grains of similar age within this sample suggests this alteration does not significantly affect the isotopic systematics of the 23.0 ± 0.7 Ma grain. Alternatively, monazite formation in this sample may relate to allanite breakdown, a process captured by the garnet during growth.

Matrix monazite grains from ET12 range from 25.3 ± 0.5 to 23.3 ± 0.8 Ma, whereas ET18b average ages of 23.4 ± 0.9 Ma. Samples ET23b and ET25 also contain 23–29 Ma monazite grains, and sample ET26 (Fig. 9) contains a 23.9 ± 0.4 Ma monazite inclusion in garnet. These ages are consistent with geochronologic studies suggesting the MCT was active at that time (e.g., Hodges et al., 1996).

7.4. Miocene (23–5 Ma): the Neohimalayan event and activation of the MCT shear zone

Miocene monazite grains, likely related to MCT activity, appear within the Greater Himalayan Crystallines as well. For example, ET18b has monazite ages that range from 21.2 ± 1.1 to 17.3 ± 0.9 Ma, ET22 contains a 19.4 ± 0.5 Ma inclusion in garnet, and sample ET25 contains a 17.9 ± 0.4 Ma matrix grain. These ages could reflect ~10–20% Pb loss from a 23 Ma grain, which could be achieved if a 100 μm monazite experienced a temperature of ~650°C for ≤5 my (Smith and Giletti, 1997).

Oligocene monazite grains are noticeably absent from rocks collected within the upper Lesser Himalaya in eastern Nepal. These samples contain several monazite grains with average ages of 13.0 ± 1.2 Ma (85H20g), 14.5 ± 0.4 Ma (ET52), and 15.5 ± 1.5 Ma (ET33). The weighted mean age of all the monazite grains these samples is 14.5 ± 0.1 Ma (24 ion microprobe spots; MSWD = 8.4). The large MSWD indicates these data do not represent a single population, probably due to analyses of various grain sizes from different structural positions. However, individual analyses suggest that the ~14 Ma age should be considered when evaluating episodes of activity within the MCT shear zone in eastern Nepal. For example, monazite grains in 85H20g are 30–50 μm in size. Thermometric calculations indicate the garnet experienced a peak temperature of 530 ± 50°C (Hubbard, 1989), within error of the minimum temperature speculated necessary to form monazite in pelitic schists (~525°C, Smith and Barreiro, 1990). The coincident thermometry as well as the protection of monazite inclusions from Pb loss by garnet shielding (Montel et al., 2000) suggest that the ~14 Ma ages obtained from sample 85H20g (Fig. 11) date their occlusion.

The ~14 Ma monazite grains appear within the Greater Himalayan Crystallines as well. For example, sample ET12 contains a 14.5 ± 0.7 Ma inclusion in garnet and two ~14 Ma matrix monazite grains. This rock was collected within a large-scale Greater Himalayan Crystallines fold and support the hypothesis that these features formed due to compression related to MCT shear zone activation during this time (e.g., Godin et al., 1999a,b). Sample ET23b, collected near the town of Ghat, contains a 15.0 ± 0.2 Ma matrix monazite grain. Rocks collected near ET23b yield anomalously young $^{40}Ar/^{39}Ar$ muscovite age (7.7 ± 0.4 Ma) and U–Th/He apatite age (0.8 ± 0.1 Ma) compared to other samples along this transect, leading Hubbard and House (2000) to propose the existence of a small-scale shear zone at this locality. The nearest structure is a normal fault within the Greater Himalayan Crystallines reported ~4 km north of ET23b (Carosi et al., 1999b).

To explore the link between MCT fault slip and leucogranite generation, we also dated monazite grains within a tourmaline-bearing High Himalayan leucogranite. Eight matrix grains in this sample (ET7) yield an average age of 20.2 ± 0.6 Ma. This ~20 Ma age is strikingly similar to those reported for the High Himalayan leucogranite from Everest (20.3 ± 0.3 Ma; Simpson et al., 2000), and elsewhere along the range front (Zanskar, India, 20.0 ± 0.5 Ma; Noble and Searle, 1995; Shishi-Pangma, eastern Nepal, 20.2 ± 0.2 Ma; Searle et al., 1997; Manaslu, central Nepal, 19.3 ± 0.3 Ma; Harrison et al., 1999b), and attest to the remarkable continuity of granite emplacement along the range front.

The youngest monazite ages reported in this study are from sample GM74 collected within the MCT shear zone in the Garhwal Himalaya (Fig. 2). This rock contains six matrix monazite grains that yield a weighted mean age of 5.9 ± 0.2 Ma (MSWD = 0.4). The grains were large (~100 μm) and at least two ion microprobe spots could be placed on each (Table 2; Fig. 12). *P–T* calculations suggest this rock experienced conditions below the closure temperature of Pb in monazite (Metcalfe, 1993; Smith and Giletti, 1997). The ~6 Ma age is similar to those found in rocks collected at the same structural location in central Nepal (Harrison et al., 1997a; Catlos et al., 2001) and indicates that post-Early Miocene activity within the MCT shear zone occurred along two transects separated by a distance of ~800 km.

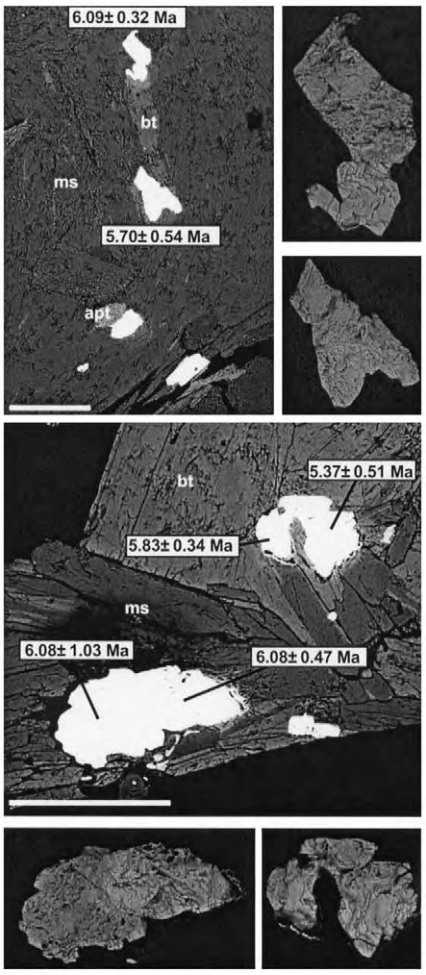

Fig. 12. Backscattered electron images of Garhwal sample GM74; ms, muscovite; bt, biotite; apt, apatite. See Fig. 2 for sample location. High contrast backscattered electron images are included for the monazites dated from GM74. The mottled texture of these grains is a consequence of interaction with the ion microprobe beam and the polish of the thin section. Th–Pb monazite ages are indicated with 1σ error. The scale bar is 200 μm.

8. Discussion: implications for the evolution of rocks within the Himalaya

We have presented in situ Th–Pb ion microprobe dating of monazite grains from rocks collected adjacent to the MCT along drainages in eastern Nepal and northwest India. The in situ method reported here has the potential to reveal more detailed information about the chronology of deformation events than those techniques that employ mineral separation (e.g., Simpson et al., 2000). For example, the monazite inclusions in garnet seen in Fig. 9 clearly illustrate the utility of an in situ technique. This garnet is so fragmented that the P-T history appears unrecoverable, but the three monazite inclusions of different age (436 ± 8, 45.8 ± 2.8, and 23.9 ± 0.4 Ma) provide a glimpse into its polyphase evolution. This could only be elucidated by directly dating each monazite grain and attaching significance to the ion microprobe spot age. The benefit of the technique increases if the thermobarometric conditions of the rock can be extracted (Fig. 8) because the timing of metamorphism can then be either directly dated or constrained.

Rocks exposed along the Dudh Kosi-Everest transect in eastern Nepal experienced several deformation events. The Phaplu augen gneiss contains Paleo-Mesoproterozoic monazite grains that represent episodes related to or preceding the assembly of the Indian subcontinent.

Table 2
Th–Pb ages of spots on individual monazite grains

High Himalayan leucogranite ET7	
Mon-sp[a]	Age[b] (Ma)
1-1	22.0 (0.4)
1-2	21.5 (0.5)
2-1	21.2 (0.3)
2-2	18.2 (0.6)
3-1	17.1 (1.3)
4-1	19.5 (0.3)
4-2	21.4 (0.4)
5-1	20.5 (0.4)

Greater Himalayan Crystallines (NMO)

ET12		ET18b		ET19		ET22		ET23b		ET25	
Mon-sp	Age (Ma)	Mon-sp	Age (Ma)	Mon-sp	Age (Ma)	Mon-sp	Age (Ma)	Mon-sp	Age (Ma)	Mon-sp	Age (Ma)
1-1[c]	14.5 (0.7)	1-1	18.6 (0.7)	1-1[c]	33.1 (0.5)	6-1	26.4 (0.7)	1-1	15.0 (0.2)	1-1	24.5 (0.5)
2-1	14.4 (0.6)	2-1	17.3 (0.9)	2-1	246 (6)	7-1[c]	19.4 (0.5)	2-1	23.4 (0.2)	2-1	23.2 (0.7)
2-2	14.9 (1.1)	3-1	19.4 (0.8)	2-2	137 (4)	8-1[c]	23.0 (0.7)	2-2	27.2 (0.3)	3-1	17.9 (0.4)
3-1	25.3 (0.5)	3-2	21.2 (1.1)	2-3	141 (2)	9-1[c]	28.1 (0.5)	2-3	23.8 (0.3)	3-2	26.0 (0.3)
3-2	24.6 (0.4)	4-1	33.5 (1.2)	4-1[c]	548 (17)	9-2[c]	27.8 (0.6)	5-1	23.7 (0.7)	4-1[c]	29.3 (1.6)
4-1	23.3 (0.8)	4-2	39.5 (0.8)	5-1	205 (3)	9-3[c]	27.1 (0.5)	6-1	29.6 (1.3)	7-1[c]	29.0 (0.5)
4-2	25.3 (0.7)	5-1	21.1 (0.9)	5-2	140 (3)					8-1[c]	28.1 (0.7)
5-1	24.4 (1.0)	7-1	19.5 (0.9)	6-1	511 (21)						
		8-1	20.2 (0.6)								
		9-1	191(2)								

Greater Himalayan Crystallines (BG), ET26	
Mon-sp	Age (Ma)
2-1	18.2 (0.4)
3-1	44.5 (0.9)
5-1[c]	23.9 (0.4)
7-1[c]	45.8 (2.8)
8-1	20.4 (0.6)
10-1[c]	436 (8)

Upper Lesser Himalaya								PAG	
ET52		ET33		85H20 g		GM74		ET38	
Mon-sp	Age (Ma)	Mon-sp	Age (Ma)	Mon-sp	Age (Ma)	Mon-sp	Age (Ma)	Mon-sp	Age (Ma)
1-1[c]	13.9 (0.5)	1-1[c]	16.4 (2.2)	1-1	10.6 (0.5)	3a-1	6.0 (0.3)	1-1	901 (13)
2-1	12.3 (0.3)	2-1	15.7 (0.7)	1-2	10.0 (0.7)	3b-1	5.7 (0.5)	1-2	1026 (28)
2-2	15.2 (0.4)	2-2	15.1 (0.3)	2-1[c]	14.2 (1.1)	4a-1	5.8 (0.3)	2-1	1646 (45)
3-1	14.6 (0.4)	2-3	15.6 (1.0)	3-1[c]	13.3 (1.7)	4a-2	5.4 (0.5)	3-1	1595 (37)
3-2	15.0 (0.3)	3a-1	14.4 (0.9)	4-1	13.3 (0.6)	4b-1	6.1 (0.5)	4-1	1648 (18)
5-1	14.8 (0.4)	3b-1	14.7 (1.8)	5-1	13.1 (1.1)	4b-2	6.1 (1.0)	4-2	1469 (38)
6-1	16.0 (0.6)	3b-2	15.3 (1.3)	7-1	16.5 (1.8)			4-3	1566 (49)
		4-1	15.1 (0.7)						
		4-2	15.7 (1.2)						
		5-1	17.1 (3.1)						

[a] The nomenclature indicates the grain and spot, respectively, of the analyzed monazite. See Figs. 2 and 3 for locations. Greater Himalayan Crystallines Namche Migmatite Orthogneiss (NMO); Greater Himalayan Crystallines Barun Gneiss (BG); Phaplu Augen Gneiss (PAG).
[b] Spot age ($\pm 1\sigma$).
[c] Monazite inclusion in garnet.

Cambro-Ordovician monazite grains are located within the Greater Himalayan Crystallines, supporting the field observations that the unit's protolith may be clastic sediments intruded by granitic bodies during Pan African orogeny (Pognante and Benna, 1993; Carosi et al., 1999a). An alternative hypothesis based on detrital zircon ages elsewhere in Nepal implies that these grains are related to Paleozoic movement along the MCT (DeCelles et al., 2000). This explanation reduces the amount of post-Eocene slip accommodated by the fault, and weakens its role in the total Indo-Asian convergence budget. Moreover, Cenozoic events along the MCT have the potential to overprint all evidence for the earlier tectonic events along that boundary. However, the ~500 Ma monazite grains were absent in the footwall lithologies in eastern Nepal, and only found within hanging wall units: the Barun Gneiss and Namche Migmatitic Orthogneiss. Petrologic observations and the location of the Pan-African monazite strongly support the explanation that the ~500 Ma grains are remnants of an intruded granite and could have acted as source material for subsequent monazite growth within the Greater Himalayan Crystallines.

The presence of ~45 Ma monazite grains within rocks of the Barun Gneiss suggests subduction of the Greater Himalayan Crystallines to conditions conducive to monazite crystallization occurred during or soon (<2 Ma) after initiation of India-Asia collision in eastern Nepal (see Rowley, 1998). The duration of the Eohimalayan event remains speculative, but the extensive presence of ~23 Ma monazite grains, consistent with estimates of timing of MCT slip reported elsewhere (e.g., Hodges et al., 1996), support a 27–32 my time span.

Since the exact location of the MCT is difficult to discern in the field, the geochemical techniques reported here provide a means to delineate the tectonic structures (see also Kohn et al., 1999). The Greater Himalayan Crystallines and lower Lesser Himalaya are distinctly differentiated based on compositional traverses along their garnets and by the presence of post-Early Miocene monazite grains. Although the P–T paths for samples reported here (Fig. 8) are subject to uncertainty because of the difficulty in evaluating the thermobarometric conditions of garnets affected by diffusion (e.g., Florence and Spear, 1991), the results agree with (1) observed mineral assemblages, (2) absence of partial-melting textures, and (3) P–T conditions of other assemblages collected nearby ($T \approx$ 550–620°C, $P \approx$ 7–8 kbar, Pognante and Benna, 1993; $T \approx$ 600–720°C, $P \approx$ 5–7 kbar, Hubbard, 1989). In addition, they illustrate the utility of the combination of thermobarometry and in situ monazite geochronology.

Both the ET52 and ET33 garnets contain monazite inclusions and record paths consistent with burial. The age of the monazite inclusion in the garnet core of ET33 is 16.2 ± 2.2 Ma, within 1σ of the 13.9 ± 0.5 Ma age of the monazite inclusion in the rim of ET52. Support for the idea that these inclusions time their occlusion by the garnet, thereby providing the paths with geochronologic constraints, comes from studies of monazite genesis that suggest that the mineral appears in pelitic rocks due to allanite breakdown at ~525°C (Smith and Barreiro, 1990) and observations that Himalayan monazite first appears coincident with the garnet isograd within the MCT shear zone (Harrison et al., 1997a,b). The potential exists that these samples experienced a garnet growth event that post-dates the monazite growth event. However, the high-grade thermobarometric conditions for ET33 and ET52, the small size of the monazite inclusions, as well as younger ages for matrix grains, suggest that Pb loss from the monazite grains would have continued until the garnet provided protection via a shielding mechanism (e.g., Montel, 1999; Montel et al., 2000). Pressure conditions recorded by the garnet rim in sample ET52, the precise age of the monazite inclusion, and a lithostatic gradient suggest the exhumation rate of the MCT shear zone in eastern Nepal is ~2 mm yr^{-1} (= 7 kbar/(0.27 kbar km^{-1} × 13.9 Ma)).

The discovery that ~7 Ma MCT footwall monazite grains (Harrison et al., 1997a; Catlos et al., 2001) are not unique to central Nepal has implications for those seeking to model Himalayan evolution and partition the amount of convergence accommodated by structures created by the India-Asia collision. For example, Guillot et al. (1999) suggests counterclockwise motion of India between 50 and 40 Ma is reflected in a delay of 10–20 my in Greater Himalaya nappe stacking from west to east across the orogen. The striking age similarity of monazite grains found at similar structural levels within the MCT footwall in the far-western and central Himalayan range suggests the influence of the Indian subcontinent's counterclockwise motion on the mechanics of convergence ceased to be discernable by the Late Miocene. Note that the inference that magmatic processes young to the east across the Himalayan orogen is also unsupported by the High Himalayan leucogranite dated in this study which yields a ~20 Ma age that corresponds remarkably well with those reported across the range front (e.g., Harrison et al., 1998, Table 1).

The age distribution and P–T conditions along the two drainages is consistent with a thermo-kinematic model in which the inverted metamorphic sequences underlying the MCT formed by the transposition of right-way-up metamorphic sequences during out-of-sequence thrusting (Harrison et al., 1998). As illustrated in Fig. 13, the MCT juxtaposes the Greater Himalayan Crystallines against the Lesser Himalaya during the Early Miocene. The Greater Himalayan Crystallines have already sustained Eohimalayan metamorphism and thickening, and monazite grains from these rocks cooling from different depths should reveal Early Miocene ages reflecting MCT activation or age gradients due to variable diffusive Pb loss. The geometry of this scenario reproduces the observed hanging wall lithostatic pressure gradient (e.g., Hubbard, 1989; Vannay and

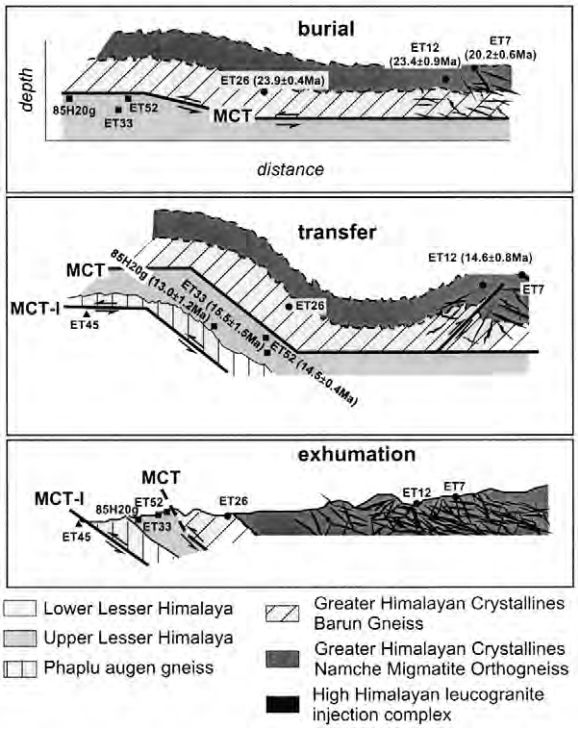

Fig. 13. Schematic illustration of the tectonic development of the Dudh Kosi-Everest Himalayan region. Faults are shown as bold lines, whereas thinner lines indicate approximate lithologic contacts. The figure illustrates the evolution of samples ET7 (circle, High Himalaya leucogranite), ET12 (circle, Greater Himalayan Crystallines), 85H20g, ET33, ET52 (square, upper Lesser Himalaya), and ET45 (triangle, lower Lesser Himalaya). During the Miocene burial stage (upper), the MCT juxtaposes the Greater Himalayan Crystallines against the upper Lesser Himalaya Formation. Miocene monazite crystallization occurs in sample ET12 and ET7. The age reported for ET12 in the upper inset is the average of Miocene monazite grains in this sample, whereas the age for ET7 is the average age of the all monazites dated in the rock. During the transfer phase at ~14 Ma (middle inset), monazite crystallization occurs within the MCT shear zone, possibly related to the transfer of deformation from the MCT to the MCT-I and other thrust planes within the shear zone. Sample ET33 records higher peak P–T conditions than sample ET52 (see Fig. 8), indicating that ET33 was transferred to deeper structural levels. Rocks that were once in the footwall of the MCT now comprise the hanging wall of the MCT-I. Monazite crystallization also occurs in sample ET12, possibly related slip along a back thrust that formed due to activity within a steepened MCT shear zone. The age reported for ET12 in the middle inset is the average of ~14 Ma monazite grains in this sample, whereas ages reported for ET33, ET52, and 85H20g are the average of all monazite grains dated in these rocks. The lower inset outlines the present-day distribution of these samples and their relationship to the MCT (see also Fig. 4). Note that sample ET45 never realized conditions conducive for monazite growth.

Hodges, 1996; Macfarlane, 1999). Additionally, the model generates the High Himalayan leucogranite injection complex by moderate amounts of shear heating (~20–30 MPa) along a thrust flat that cuts through Indian rocks.

The model assumes that when slip on the MCT ceased, the MBT activated, causing the MCT ramp to subsequently rotate (Fig. 13, middle inset). During the Late Miocene, slip along the MCT-I began, transferring footwall rocks (i.e. upper Lesser Himalaya) to the hanging wall. If conditions were conducive to monazite growth during these events, upper Lesser Himalayan grains should record post-Early Miocene ages. Analysis of 24 monazite grains from three eastern Nepal upper Lesser Himalaya samples yield a weighted mean age of 14.5 ± 0.1 Ma, whereas Garhwal sample GM74 contains ~6 Ma monazite grains. These ages should be considered when evaluating episodes of MCT shear zone activity in eastern Nepal and northwest India.

The youngest monazite grain analyzed along the Dudh Kosi-Everest transect yields a Th–Pb age of 10.3 ± 0.8 Ma (two spots; ~74% radiogenic ^{208}Pb). Although 7–3 Ma monazite ages were absent in the rocks analyzed from this area, this does not preclude the Harrison et al. (1998) model as a viable explanation for the metamorphic evolution of the orogen (see Fig. 13). The nappe structure in eastern Nepal likely obscures the reactivated ramp equivalent exposed in central Nepal. We emphasize that in central Nepal and the Garhwal Himalaya, Late Miocene monazite grains are found near the MCT-I. However, the correlative structural level is inaccessible in eastern Nepal due to burial beneath the nappe. Along this transect, allanite is the dominant accessory mineral until <1 km beneath the sillimanite isograd, where monazite appears. Attempts at dating allanite grains from this locale have the potential to reveal further details of the history of the MCT shear zone.

Folds within the Greater Himalayan Crystallines has been thought to be due to gravity sliding along the STDS (e.g., Burchfiel et al., 1992), but the presence of ~23 and ~14 Ma monazite grains in sample ET12, collected with one of these large-scale structures along the Dudh Kosi-Everest transect (Fig. 3), requires an alternative hypothesis. Analog models intended to simulate continental convergence as seen in profile suggest the shape of an orogen is strongly influenced by the geometry of the indenter (Bonini et al., 1999). The experiments support the idea that progressive shortening within the MCT shear zone combined with the steepening MCT ramp, as proposed by Harrison et al. (1998), could account for fold formation in the Greater Himalayan Crystallines (Fig. 13; middle inset). The monazite ages reported here from eastern Nepal are consistent with the concept that folds within the Greater Himalayan Crystallines relate to post-Early Miocene activation of the MCT.

9. Conclusions

This study attempts to decipher aspects of the deformation chronology of the Himalaya by using in situ Th–Pb ion microprobe dating of monazite grains from samples collected roughly perpendicular to the MCT along two river drainages: the Bhagirathi River, Garhwal Himalaya, India, and the Dudh Kosi, south of Mt. Everest, Nepal. Paleo-Mesoproterozoic monazite grains are found in an augen gneiss unit collected within the MCT shear

Table 3
Summary of the Monazite Ages

Sample[a]	Average age (Ma) ($\pm\sigma$)	Weighted mean age (Ma) ($\pm\sigma$)	MSWD[b]
ET7	20.2 (0.6)	20.7 (0.1)	8.6
ET12	20.8 (0.8)	21.9 (0.2)	62
ET18b[c]	23.4 (0.9)	22.7 (0.3)	81
ET19	245 (10)	49.1 (0.5)	1375
ET22	25.3 (0.6)	25.3 (0.2)	43
ET23b	25.7 (0.9)	22.1 (0.1)	265
ET25	25.4 (0.8)	24.4 (0.2)	76
ET26[c]	20.8 (0.5)	20.9 (0.3)	33
ET33	15.5 (1.5)	15.2 (0.2)	0.3
ET38	1407 (35)	1219 (9)	250
ET52	14.5 (0.4)	14.5 (0.1)	11
GM74	5.86 (0.58)	5.88 (0.18)	0.4
85H20 g	13.0 (1.2)	11.8 (0.3)	5.6

[a] See Fig. 3 for sample locations, and Table 2 for individual spot analyses. All ages are reported with 1σ uncertainty.
[b] Mean square weighted deviation calculated using 1σ errors.
[c] Calculations exclude some analyses. ET18b age summary excludes monazite 9-1. Summary for ET26 includes only the Miocene monazite ages.

zone, whereas high-grade hanging wall garnets retain Cambro-Ordovician monazite inclusions. The extensive presence of ~23 Ma monazite grains in hanging wall rocks indicate that the unit was metamorphosed during MCT slip following ~30 my of Eohimalayan crustal thickening. Upper Lesser Himalayan monazite inclusions in garnet record a clear signature at 14.5 ± 0.1 Ma, whereas the ~23 Ma signal that characterizes hanging wall rocks is notably absent. The ~14 Ma age is found in rocks collected within a large scale Greater Himalayan Crystallines fold, consistent with the hypothesis that these structures formed due to slip along a steepened MCT ramp.

Garnets from the MCT hanging wall (the Greater Himalayan Crystallines) and footwall (lower Lesser Himalaya) show fundamental differences in compositional zoning of Mn, Ca, Mg, and Fe. P–T paths consistent with burial are obtained from two upper Lesser Himalaya samples. The garnet grains contain monazite inclusions, and suggest the utility of combining thermobarometry and in situ geochronology. The age data reported here are consistent with the Harrison et al. (1998) model in which the inverted metamorphic sequence underlying the MCT formed by the transposition of right-way-up metamorphic sequences during post-Early Miocene shearing. The youngest monazite ages (5.9 ± 0.2 Ma) are matrix grains located within the MCT shear zone along the Bhagirathi River, Garhwal region, India, and are similar to those reported for monazite at similar structural levels in central Nepal (e.g., Harrison et al., 1997a). The striking continuity of orogenic events within the range is further manifested by the ~20 Ma age of a High Himalayan leucogranite collected from an injection complex along the Dudh Kosi-Everest transect, resembling ages of these bodies elsewhere. The geochronologic and thermobarometric information documented here provides clear quantitative constraints for those seeking to decipher the evolution of the Himalayan orogen, and suggests that in situ methods are the ideal means of evaluating the history of an orogen that has experienced a lengthy and complex sequence of tectonic events.

Acknowledgements

Funding from the National Science Foundation supported this project, and we acknowledge facility support from the Instrumentation and Facilities Program of the National Science Foundation. We thank Karen McBride for field assistance and Chris Coath for help with ion microprobe analysis. We are particularly grateful to Mike Searle for supplying the Garhwal Himalaya samples from the collection of R.P. Metcalfe. The manuscript benefited greatly from comments by Calvin Miller and an anonymous reviewer.

References

Ahmad, T., Mukherjee, P.K., Trivedi, J.R., 1999. Geochemistry of Precambrian mafic magmatic rocks of the Western Himalaya, India: petrogenetic and tectonic implications. Chemical Geology 160, 103–119.

Ahmad, T., Harris, N., Bickle, M., Chapman, H., Bunbury, J., Prince, C., 2000. Isotopic constraints on the structural relationships between the Lesser Himalayan Series and High Himalayan Crystalline Series, Garhwal Himalaya. Geological Society of America Bulletin 112, 467–477.

Akiba, C., Amma, S., Ohta, Y., 1973. Arun River region. In: Hashimoto, S. (Ed.). Geology of the Nepal Himalayas. Saikon Publishing Company, Japan, pp. 13–31.

Amma, S., Akiba, C., 1967. Geology of the area along the Arun River and Dudh Kosi, east Nepal. Journal of the Geological Society of Japan 73, 369–376.

Argles, T.W., Prince, C.I., Foster, G.L., Vance, D., 1999. New garnets for old? Cautionary tales from young mountain belts. Earth and Planetary Science Letters 172, 301–309.

Arita, K., 1983. Origin of the inverted metamorphism of the Lower Himalaya, central Nepal. Tectonophysics 95, 43–60.

Armijo, R., Tapponnier, P., Mercier, J.L., Tonglin, H., 1989. Quaternary

extension in southern Tibet: field observations and tectonic implications. Journal of Geophysical Research 91, 13,803–13,872.

Auden, M.A., 1937. The structure of the Himalaya in Garhwal. Records of the Geological Survey of India 71, 407–433.

Balasubramaniyam, M.N., Murthy, M.K., Paul, D.K., Sarkar, A.K., 1978. K-Ar ages of Indian kimberlites. Journal of Geological Society of India 19, 548–585.

Berman, R.G., 1990. Mixing properties of Ca-Mg-Fe-Mn garnets. American Mineralogist 75, 328–344.

Bhargava, O.N., Bassi, U.K., 1994. The crystalline thrust sheets of the Himachal Himalaya and the age of amphibolite facies metamorphism. Journal of the Geological Society of India 43, 343–352.

Bhatia, S.C., Kumar, M.R., Gupta, H.K., 1999. A probabilistic seismic hazard map of India and adjoining regions. Annali di Geofisica 42, 1153–1164.

Bonini, M., Sokoutis, D., Talkbot, C.J., Boccaletti, M., Milnes, A.G., 1999. Indenter growth in analogue models of alpine-type deformation. Tectonics 18, 119–128.

Bordet, P., 1961. In: Recherches geologiques dans l'Himalaya du Nepal, region du Makalu. Centre National de la Recherches Scientifiques, Paris (275pp.).

Brunel, M., Kienast, J.R., 1986. Etude pétro-structurale des chevauchements ductiles himalayens sur la transversale de l'Everest-Makalu (Nepal oriental). Canadian Journal of Earth Sciences 23, 1117–1137.

Burchfiel, C.B., Zhiliang, C., Hodges, K.V., Yuping, L., Royden, L.H., Changrong, D., Jiene, X., 1992. The Southern Tibetan detachment system Himalayan orogen: extension contemporaneous with and parallel to shortening in a collisional mountain belt. United States Geological Survey Special Paper 269, 1–40.

Burg, J.P., Brunel, M., Gapais, D., Chen, G.M., Liu, G.H., 1984. Deformation of leucogranites of the crystalline Main Central Sheet in southern Tibet (China). Journal of Structural Geology 6, 535–542.

Carosi, R., Musumeci, G., Pertusati, P.C., 1996. Southward extensional tectonics and dike emplacement in the High Himalayan Crystallines of Khumbu Himal, eastern Nepal. In: 11th Himalaya–Karakorum–Tibet Workshop, Abstract Volume, Flagstaff, Arizona, p. 28.

Carosi, R., Lombardo, B., Molli, G., Musumeci, G., Pertusati, P.C., 1998. The South Tibetan Detachment System in the Rongbuk valley, Everest region. Deformation and geological implications. Journal of Asian Earth Sciences 16, 299–311.

Carosi, R., Lombardo, B., Musumeci, G., Pertusati, P.C., 1999a. Geology of the Higher Himalayan Crystallines in Khumbu Himal (eastern Nepal). Journal of Asian Earth Sciences 17, 785–803.

Carosi, R., Musumeci, G., Pertusati, P.C., 1999b. Extensional tectonics in the higher Himalayan crystallines of Khumbu Himal, Eastern Nepal. Himalaya and Tibet: Mountain Roots to Mountain Tops, Macfarlane, A., Sorkhabai, R.B., Quade, J. (Eds.). Geological Society of America Special Paper 328, 211–223.

Catlos, E.J., Harrison, T.M., Grove, M., Kohn, M.J., Upreti, B.N., 1999. Evidence for Pliocene Activity across the Main Central Thrust Shear Zone, central Nepal. American Geophysical Union Fall Meeting Abstracts, F1016.

Catlos, E.J., Sorensen, S.S., Harrison, T.M., 2000. Th-Pb ion-microprobe dating of allanite. American Mineralogist 85, 633–648.

Catlos, E.J., Harrison, T.M., Kohn, M.J., Grove, M., Ryerson, F.J., Manning, C.E., Upreti, B.N., 2001. Geochronologic and thermobarometric constraints on the evolution of the Main Central Thrust, central Nepal Himalaya. Journal of Geophysical Research. (in press).

Chen, Z., Burchfiel, B.C., Liu, Y., King, R.W., Royden, L.H., Tang, W., Wang, E., Zhao, J., Zhang, X., 2000. Global Positioning System measurements from eastern Tibet and their implications for India/Eurasia intercontinental deformation. Journal of Geophysical Research 105, 16,215–16,277.

Colchen, M., Le Fort, P., Pêcher, A., 1980. Annapurna-Manaslu-Ganesh Himal. In: Centre National de la Recherches Scientifiques, Paris, (136pp.).

Coleman, M.E., 1998. U–Pb constraints on Oligocene–Miocene deformation and anatexis within the central Himalaya, Marsyandi Valley, Nepal. American Journal of Science 298, 553–571.

Davidson, C., Grujic, D.E., Hollister, L.S., Schmid, S.M., 1997. Metamorphic reactions related to decompression and synkinematic intrusion of leucogranite, High Himalayan Crystallines, Bhutan. Journal of Metamorphic Geology 15, 593–612.

DeCelles, P.G., Gehrels, G.E., Quade, J., LaReau, B., Spurlin, M., 2000. Tectonic implications of U–Pb zircon ages of the Himalayan orogenic belt in Nepal. Science 288, 497–499.

DeMets, C., Gordon, R.G., Argus, D.F., Stein, S., 1990. Current plate motions. Geophysical Journal International 101, 425–478.

Dickenson, M.P., Hewitt, D., 1986. A garnet–chlorite geothermometer. Geological Society of America Abstracts with Programs 18, 584.

Duppert, L., Dissler, E., Dore, F., Gresselin, F., Gall, J.K., 1990. Cadomian geodynamic evolution of the north-eastern Armorian Massif (Normandy and Maine). The Cadomian Orogeny, D'Lemos, R.S., Strachan, R.A., Topley, C.G. (Eds.). Geological Society of London 51, 115–131.

England, P., Le Fort, P., Molnar, P., Pêcher, A., 1992. Heat sources for Tertiary metamorphism and anatexis in the Annapurna-Manaslu region, central Nepal. Journal of Geophysical Research 97, 2107–2128.

Ernst, W.G., 1973. Blueschist metamorphism and P-T regimes in active subduction zones. Tectonophysics 17, 255.

Ferrara, G., Lombardo, B., Tonarini, S., 1983. Rb/Sr geochronology of granites and gneisses from the Mount Everest Region, Nepal Himalaya. Geologische Rundschau 72, 119–136.

Ferry, J.M., Spear, F.S., 1978. Experimental calibration of partitioning of Fe and Mg between biotite and garnet. Contributions to Mineralogy and Petrology 66, 113–117.

Finger, F., Broska, I., Roberts, M.P., Schermaier, A., 1998. Replacement of primary monazite by apatite-allanite-epidote coronas in an amphibolite facies granite gneiss from the eastern Alps. American Mineralogist 83, 248–258.

Florence, F.P., Spear, F.S., 1991. Effects of diffusional modification of garnet growth zoning on P–T path calculations. Contributions to Mineralogy and Petrology 107, 487–500.

Foster, G.L., 2000. The pre-Neogene thermal history of the Nanga Parbat Haramosh Massif and the NW Himalaya. PhD dissertation, The Open University, United Kingdom (345pp.).

Foster, G., Kinny, P., Vance, D., Prince, C., Harris, N., 2000. The significance of monazite U–Th–Pb age data in metamorphic assemblages; a combined study of monazite and garnet chronometry. Earth and Planetary Science Letters 181, 327–340.

Fuchs, G.R., 1968. In: The geological history of the Himalayas. Report of the 22nd International Geological Congress, 3, pp. 161–174.

Gansser, A., 1964. The geology of the Himalayas. Wiley, New York (289pp.).

Garzanti, E., Casnedi, R., Jadoul, F., 1986. Sedimentary evidence of a Cambro-Ordovician orogenic event in the Northwestern Himalaya. Sedimentary Geology 48, 237–265.

Godin, L., Brown, R.L., Hanmer, S., Parrish, R.R., 1999a. Back folds in the Himalayan orogen: an alternative interpretation. Geology 27, 151–154.

Godin, L., Brown, R.L., Hanmer, S., 1999b. High strain zone in the hanging wall of the Annapurna detachment, central Nepal Himalaya. Himalaya and Tibet: Mountain Roots to Mountain Tops, Macfarlane, A., Sorkhabi, R.B., Quade, J. (Eds.). Geological Society of America Special Paper 328, 199–210.

Graham, C.M., England, P., 1976. Thermal regimes and regional metamorphism in the vicinity of overthrust faults: an example of shear heating and inverted metamorphic zonation from southern California. Earth and Planetary Science Letters 31, 142–152.

Grujic, D., Grasemann, B., Vannay, J-C., 1999. Extrusion of tectonic wedges as a process of exhumation: Which models fit the field data from the High Himalayan Crystalline? In: 14th Himalaya–Karakoram–Tibet Workshop, Kloster Ettal Germany, Terra Nostra, 99/2, pp. 60–62.

Guillot, S., Cosca, M., Allemand, P., Le Fort, P., 1999. Contrasting metamorphic and geochronologic evolution along the Himalayan belt.

Himalaya and Tibet: Mountain Roots to Mountain Tops, Macfarlane, A., Sorkhabai, R.B., Quade, J. (Eds.). Geological Society of America Special Paper 328, 117–128.

Hagen, T., 1968. In: Report on the geological survey of Nepal: Volume 1, Preliminary reconnaissance. Schweizerische Naturforschende Gesellschaft Denkschriften Mémoires (160pp.).

Harrison, T.M., McKeegan, K.D., Le Fort, P., 1995. Detection of inherited monazite in the Manaslu leucogranite by $^{208}Pb/^{232}Th$ ion microprobe dating: Crystallization age and tectonic implications. Earth and Planetary Science Letters 133, 271–282.

Harrison, T.M., Ryerson, F.J., Le Fort, P., Yin, A., Lovera, O.M., Catlos, E.J., 1997a. A Late Miocene-Pliocene origin for central Himalayan inverted metamorphism. Earth and Planetary Science Letters 146, E1–E8.

Harrison, T.M., Grove, M., Lovera, O.M., 1997b. New insights into the origin of two contrasting Himalayan granite belts. Geology 25, 899–902.

Harrison, T.M., Grove, M., Lovera, O.M., Catlos, E.J., 1998. A model for the origin on Himalayan anatexis and inverted metamorphism. Journal of Geophysical Research 103, 27,017–27,032.

Harrison, T.M., Grove, M., Lovera, O.M., Catlos, E.J., D'Andrea, J., 1999a. The origin of Himalayan anatexis and inverted metamorphism: models and constraints. Journal of Asian Earth Sciences 17, 755–772.

Harrison, T.M., Grove, M., McKeegan, K.D., Coath, C.D., Lovera, O.M., Le Fort, P., 1999b. Origin and emplacement of the Manaslu intrusive complex, Central Himalaya. Journal of Petrology 40, 3–19.

Hodges, K.V., 2000. Tectonics of the Himalaya and southern Tibet from two perspectives. Geological Society of America Bulletin 112, 324–350.

Hodges, K.V., Parrish, R.R., Housh, T.B., Lux, D.R., Burchfiel, B.C., Royden, L.H., Chen, Z., 1992. Simultaneous Miocene extension and shortening in the Himalayan orogen. Science 258, 1466–1470.

Hodges, K.V., Burchfiel, B.C., Royden, L.H., Chen, Z., Liu, Y., 1993. The metamorphic signature of contemporaneous extension and shortening in the central Himalayan orogen: Data from the Nyalam transect, southern Tibet. Journal of Metamorphic Geology 11, 721–737.

Hodges, K.V., Parrish, R.R., Searle, M.P., 1996. Tectonic evolution of the central Annapurna Range, Nepalese Himalayas. Tectonics 15, 1264–1291.

Hoisch, T.D., 1990. Empirical calibration of six geobarometers for the mineral assemblage quartz + muscovite + biotite + plagioclase + garnet. Contributions to Mineralogy and Petrology 104, 225–234.

Hubbard, M.S., 1988. Thermobarometry, $^{40}Ar/^{39}Ar$ geochronology, and structure of the Main Central Thrust Zone and Tibetan Slab, eastern Nepal Himalaya. PhD dissertation, Massachusetts Institute of Technology, 169 pp.

Hubbard, M.S., 1989. Thermobarometric constraints on the thermal history of the Main Central Thrust Zone and Tibet Slab, eastern Nepal Himalaya. Journal of Metamorphic Geology 7, 19–30.

Hubbard, M.S., 1996. Ductile shear as a cause of inverted metamorphism: Example from the Nepal Himalaya. Journal of Geology 104, 493–499.

Hubbard, M.S., Harrison, T.M., 1989. $^{40}Ar/^{39}Ar$ age constraints on deformation and metamorphism in the Main Central Thrust zone and Tibetan Slab, eastern Nepal Himalaya. Tectonics 8, 865–880.

Hubbard, M.S., House, M., 2000. Low temperature dating of high mountain rocks: (U–Th)/He ages from Higher Himalayan samples, eastern Nepal. In: 15th Himalaya–Karakoram–Tibet Workshop, Chengdu, China, Earth Science Frontiers 7 supplement, pp. 16–17.

Huerta, A.D., Royden, L.H., Hodges, K.V., 1996. The interdependence of deformational and thermal processes in mountain belts. Science 273, 637–639.

Kai, K., 1981. Rb–Sr ages of the biotite and muscovite of the Himalaya, eastern Nepal; its implication in the uplift history. Geochemical Journal 15, 63–68.

Kaneko, Y., 1995. Thermal structure in the Annapurna region, central Nepal Himalaya: Implication for the inverted metamorphism. Journal of Mineralogy, Petrology, and Economic Geology 90, 143–154.

Kaneoka, I., Kono, M., 1981. $^{40}Ar/^{39}Ar$ dating of Himalayan rocks from the Mount Everest Region. Journal of Geophysics 49, 207–211.

Klootwijik, C.T., Conaghan, P.J., Powell, C.M., 1985. The Himalayan arc: Largescale continental subduction, oroclinal bending, and backarc spreading. Earth and Planetary Science Letters 75, 167–183.

Kohn, M.J., Spear, F.S., 2001. Retrograde net transfer reaction (ReNTR) insurance for P–T estimates. Geology 28, 1127–1130.

Kohn, M.J., Catlos, E.J., Ryerson, F.J., Harrison,T.M., 1999. Metamorphic P–T discontinuity at the base of the MCT zone, central Nepal. In: American Geophysical Union, Fall Meeting Abstracts Volume, F991.

Laird, J., 1988. Chlorites: metamorphic petrology. Hydrous Phyllosilicates (Exclusive of Micas), Bailey, S.W. (Ed.). Mineralogical Society of America Reviews in Mineralogy 19, 405–453.

Le Fort, P., 1975. Himalaya, the collided range, Present knowledge of the continental arc. American Journal of Science 275A, 1–44.

Le Fort, P., 1996. Evolution of the Himalaya. In: Yin, A., Harrison, T.M. (Eds.). The Tectonic Evolution of Asia. Cambridge University Press, Cambridge, pp. 95–109.

Le Fort, P., Debon, F., Pêcher, A., Sonet, A.V.P., 1986. The 500 Ma magmatic event in alpine southern Asia, a thermal episode at Gondwana scale. Évolution des domains orogéniques d'Asie méridionale (de la Turquie à l'Indoneasie), Le Fort, P., Colchen, M., Montenat, C. (Eds.). Science de la Terre 47, 191–209.

Lombard, A., 1952. La tectonique du massif de l'Everest, partie occidentale; note preliminaire. Archives des Sciences, Societe de Physique et d'Histoire Naturelle de Geneve 5, 403–405.

Lombardo, B., Rolfo, F., 2000. Two contrasting eclogite types in the Himalayas: Implications for the Himalayan orogeny. Journal of Geodynamics 30, 37–60.

Lombardo, B., Pertusati, P., Borghi, S., 1993. Geology and tectonomagmatic evolution of the eastern Himalaya along the Chomolungma-Makalu transect. Himalayan Tectonics, Trealor, P.J., Searle, M.P. (Eds.). Geological Society Special Publication 74, 341–355.

Macfarlane, A.M., 1999. The metamorphic history of the crystalline rocks in the high Himalaya, Nepal: insights from thermobarometric data. Journal of Asian Earth Sciences 17, 741–753.

Manickavasagam, R.M., Jain, A.K., Singh, S., Asokan, A., 1999. Metamorphic evolution of the northwest Himalaya, India: Pressure-temperature data, inverted metamorphism, and exhumation in the Kashmir, Himachal, and Garhwal Himalayas. Himalaya and Tibet: Mountain Roots to Mountain Tops, Macfarlane, A., Sorkhabai, R.B., Quade, J. (Eds.). Geological Society of America Special Paper 328, 179–198.

Mazumder, R., Bose, P.K., Sarkar, S., 2000. A commentary on the tectonosedimentary record of the pre-2.0 Ga continental growth of India via-à-vis a possible pre-Gondwana Afro-Indian supercontinent. Journal of African Earth Sciences 30, 201–217.

Medicott, H.B., 1864. On the geologic structure and relations of the southern portion of the Himalayan range between the rivers Ganges and Ravee. Memoirs of the Geologic Survey of India 3, 1–206.

Meigs, A.J., Burbank, D.W., Beck, R.A., 1995. Middle-late Miocene [>10 Ma] formation of the Main Boundary Thrust in the Western Himalaya. Geology 23, 423–426.

Meldrum, A., Boatner, L.A., Weber, W.J., Ewing, R.C., 1998. Radiation damage in zircon and monazite. Geochimica et Cosmochimica Acta 62, 2509–2520.

Metcalfe, R.P., 1993. Pressure, temperature and time constraints on metamorphism across the Main Central Thrust zone and High Himalaya Slab in the Garhwal Himalaya. Himalayan Tectonics, Trealor, P.J., Searle, M.P. (Eds.). Geological Society Special Publication 74, 485–509.

Middlemiss, C.S., 1885. A fossiliferous series in the Lower Himalaya, Garhwal and Kumaon. Records of the Geological Survey of India 18, 73–77.

Middlemiss, C.S., 1887. Physical geology of West British Garhwal; with notes on a route traverse through Jaunsar Bawar and Tiri-Garhwal. Records of the Geological Survey of India 20, 26–40.

Middlemiss, C.S., 1888. Crystalline and metamorphic rocks of the lower

Himalaya, Garhwal and Kuamon, section III. Records of the Geological Survey of India 21, 11–28.
Minster, J.B., Jordan, T.H., 1978. Present-day plate motions. Journal of Geophysical Research 83, 5331–5354.
Mishra, D.C., 1992. Mid-continent gravity high of central India and the Gondwana tectonics. Tectonophysics 212, 153–161.
Montel, J., 1999. Some good reasons for monazite to be concordant. In: European Union of Geosciences Journal of Conference Abstracts, 10, p. 800.
Montel, J., Kornprobst, J., Vielzeuf, D., 2000. Preservation of old U-Th-Pb ages in shielded monazite: example from Beni Bousera Hercynian kinzigites (Morocco). Journal of Metamorphic Geology 18, 335–342.
Mugnier, J.L., Leturmy, P., Mascle, G., Huyghe, P., Chalaron, E., Vidal, G., Husson, L., Delcaillau, B., 1999. The Siwaliks of western Nepal, I. Geometry and kinematics. Journal of Asian Earth Sciences 17, 629–642.
Nelson, K.D., Zhao, W., Brown, L.D., Project, I.N.D.E.P.T.H., 1996. Partially molten crust beneath Southern Tibet: synthesis of project INDEPTH results. Science 274, 1684–1688.
Noble, S.R., Searle, M.P., 1995. Age of crustal melting and leucogranite formation from U-Pb zircon and monazite dating in the western Himalaya, Zanskar, India. Geology 23, 1135–1138.
Oldham, R.D., 1883. Note on the geology of Jaunsar and the lower Himalayas. Memoirs of the Geological Survey of India 3, 193–198.
Patzelt, A., Huami, L., Wang, J., Appel, E., 1996. Palaeomagnetism of Cretaceous to Tertiary sediments from southern Tibet: evidence for the extent of the northern margin of India prior to the collision with Eurasia. Tectonophysics 259, 259–284.
Pêcher, A., 1989. The metamorphism in the central Himalaya. Journal of Metamorphic Geology 7, 31–41.
Pêcher, A., Scaillet, B., 1989. La structure du Haut-Himalaya au Garhwal (Indes). Eclogae Geologicae Helveticae 82/2, 655–668.
Pilgrim, G.E., West, W.D., 1928. The structure and correlation of the Simla Rocks. Memoirs of the Geological Survey of India LIII, 1–138.
Pognante, U., Benna, P., 1993. Metamorphic zonation, migmitization and leucogranites along the Everest transect of Eastern Nepal and Tibet: record of an exhumation history. Himalayan Tectonics, Trealor, P.J., Searle, M.P. (Eds.). Geological Society Special Publication 74, 323–340.
Qureshy, M.N., Iqbaluddin, 1992. A review of the geophysical constraints in modelling the Gondwana crust in India. Tectonophysics 212, 141–151.
Rabi, D., Chantraine, J., Chauvel, J.J., Dens, E., Bale, P., Bardz, P., 1990. The Briovernian (Upper Proterozoic) and Cadomian Orogeny in the Armorian massif. The Cadomian Orogeny, D'Lemos, R.S., Strachan, R.A., Topley, C.G. (Eds.). Geological Society of London 51, 81–94.
Radhakrishana, B.P., 1989. Suspect tectono-stratigraphic terrane elements in the Indian subcontinent. Journal of the Geological Society of India 4, 1–24.
Rao, D.A., Ram Babu, H.V., Sivakumar Sinha, G.D.J., 1992. Crustal structure associated with Gondwana graben across the Narmada-Son lineament in India: an inference from aeromagnetics. Tectonophysics 212, 153–161.
Ray, S., 1947. Zonal metamorphism in the eastern Himalayas and some aspects of local geology. Quarterly Journal of the Geological, Mining and Metallurgical Society of India 19, 117–140.
Reddy, V.D., Prasad, C.V.R.K., 1979. Paleomagnetism of the dykes from Kolar gold Mines. Journal of the Geological Society of India 20, 489–500.
Rowley, D.B., 1996. Age of initiation of collision between India and Asia: A review of the stratigraphic data. Earth and Planetary Science Letters 145, 1–13.
Rowley, D.B., 1998. Minimum age of initiation of collision between India and Asia north of Everest based on the subsidence history of the Zhepure mountain section. Journal of Geology 106, 229–235.
Royer, J.Y., Sandwell, D.T., 1989. Evolution of the eastern Indian Ocean since the Late Cretaceous: Constraints from Geosat altimetry. Journal of Geophysical Research 94, 13755–13782.
Schärer, U., 1984. The effect of initial ^{230}Th disequilibrium on young U–Pb ages: the Makalu case. Earth and Planetary Science Letters 67, 191–204.
Schärer, U., Xu, R.H., Allegre, C.J., 1986. U–(Th) –Pb systematics and ages of Himalayan leucogranites, South Tibet. Earth and Planetary Science Letters 77, 35–48.
Schelling, D., 1992. The tectonostratigraphy and structure of the eastern Nepal Himalaya. Tectonics 11, 925–943.
Schneider, E., Aerberli, S., Fuerer, H., Gürtler, R., Jenny, R., Schriebl, H., 1981a. Dudh Kosi 1:50,000. Research Scheme Nepal Himalaya (Eds.), GEO-Buch Verlag, Kartographische Anstalt Freytag-Berndt und Artaira, Vienna.
Schneider, E., Aerberli, S., Fuerer, H., Gürtler, R., Jenny, R., Schriebl, H., 1981b. Shrong/Hinku 1:50,000. Research Scheme Nepal Himalaya (Eds.), GEO-Buch Verlag, Kartographische Anstalt Freytag-Berndt und Artaira, Vienna.
Schneider, E., Aerberli, S., Fuerer, H., Gürtler, R., Jenny, R., Schriebl, H., 1981c. Khumbu Himal 1:50,000. Research Scheme Nepal Himalaya (Eds.), GEO-Buch Verlag, Kartographische Anstalt Freytag-Berndt und Artaira, Vienna.
Searle, M.P., 1999. Extensional and compressional faults in the Everest-Lhotse massif, Khumbu Himalaya, Nepal. Journal of the Geological Society, London 156, 227–240.
Searle, M.P., Rex, D.C., 1989. Thermal model for the Zanskar Himalaya. Journal of Metamorphic Geology 7, 127–134.
Searle, M.P., Metcalfe, R.P., Rex, A.J., Norry, M.J., 1993. Field relations, petrogenesis and emplacement of the Bhagirathi leucogranite, Garhwal Himalayas. Himalayan Tectonics, Trealor, P.J., Searle, M.P. (Eds.). Geological Society Special Publication 74, 429–444.
Searle, M.P., Parrish, R.R., Hodges, K.V., Hurford, A.J., Ayres, M.W., Whitehouse, M.J., 1997. Shisha-Pangma leucogranite, South Tibetan Himalaya: Field relations, geochemistry, age, origin, and emplacement. Journal of Geology 105, 295–317.
Searle, M.P., Noble, S.R., Hurford, A.J., Rex, D.C., 1999. Age of crustal melting, emplacement and exhumation history of the Shivling leucogranite, Garhwal Himalaya. Geological Magazine 136, 513–525.
Seeber, L., Armbruster, J.G., Quittmeyer, R., 1981. Seismicity and continental subduction in the Himalayan arc. Zagros, Hindu Kush, Himalayan Geodynamic Evolution, Gupta, H.K., Delany, F.M. (Eds.). American Geophysical Union 3, 215–242.
Shen, Z-K., Zhao, C., Yin, A., Li, Y., Jackson, D.D., Fang, P., Dong, D., 2000. Contemporary crustal deformation in east Asia constrained by global positioning system measurements. Journal of Geophysical Research 105, 5721–5734.
Simpson, R.L., Parrish, R.R., Searle, M.P., Waters, D.J., 2000. Two episodes of monazite crystallization during metamorphism and crustal melting in the Everest region of the Nepalese Himalaya. Geology 28, 403–406.
Smith, A.G., 1999. Gondwana: its shape, size and position from Cambrian to Triassic times. Journal of African Earth Sciences 28, 71–97.
Smith, H.A., Barreiro, B., 1990. Monazite U–Pb dating of staurolite grade metamorphism in pelitic schists. Contributions to Mineralogy and Petrology 105, 602–615.
Smith, H.A., Giletti, B.J., 1997. Lead diffusion in monazite. Geochimica et Cosmochimica Acta 61, 1047–1055.
Spear, F.S., 1991. On the interpretation of peak metamorphic temperatures in light of garnet diffusion during cooling. Journal of Metamorphic Geology 9, 379–388.
Spear, F.S., 1993. Metamorphic phase equilibria and pressure–temperature–time paths. Mineralogical Society of America (799pp.).
Spear, F.S., Peacock, S.M., 1989. In: Metamorphic pressure-temperature-time paths. American Geophysical Union Short Course in Geology, 7, p. 102.
Spear, F.S., Kohn, M.J., Florence, F., Menard, T., 1990. A model garnet and plagioclase growth in pelitic schists: implications for thermobarometry

and P–T path determinations. Journal of Metamorphic Geology 8, 683–696.

Spear, F.S., Kohn, M.J., Paetzold, S., 1995. Petrology of the regional sillimanite zone, west-central New Hampshire, USA, with implications for the development of inverted isograds. American Mineralogist 80, 361–376.

St-Onge, M., 1987. Zoned poikiloblastic garnets: P–T paths and syn-metamorphic uplift through 30 km of structural depth, Wopmay Orogen, Canada. Journal of Petrology 28, 1–21.

Tripathi, C., Singh, G., 1987. Gondwana and associated rocks of the Himalaya and their significance. Gondwana Six; Stratigraphy, sedimentology, and paleontology, McKenzie, G.D. (Ed.). American Geophysical Union Geophysical Monograph 41, 195–205.

Upreti, B.N., 1999. An overview of the stratigraphy and tectonics of the Nepal Himalaya. Journal of Asian Earth Sciences 17, 741–753.

Vance, D., Harris, N., 1999. The timing of prograde metamorphism in the Zanskar Himalaya. Geology 27, 395–398.

Walker, J.D., Martin, M.W., Bowring, S.A., Searle, M.P., Waters, D.J., Hodges, K.V., 1999. Metamorphism, melting, and extension: age constraints from the High Himalayan slab, S.E. Zanskar, N.W. Lahoul. Journal of Geology 107, 473–495.

Valdiya, K.S., 1980. Geology of the Kumaun Lesser Himalaya. Wadia Institute of Himalayan Geology (291pp.).

Valdiya, K.S., 1992. The Main Boundary Thrust Zone of the Himalaya. India. Annales Tectonicae 6, 54–84.

Valdiya, K.S., 1993. Evidence for Pan-African-Cadomian tectonic upheavals in the Himalaya. Journal of the Palaeontological Society of India 38, 51–62.

Valdiya, K.S., 1995. Proterozoic sedimentation and Pan-African geodynamic development in the Himalaya. Precambrian Research 74, 35–55.

Vannay, J.-C., Grasemann, B., 1998. Inverted metamorphism in the High Himalaya of Himachal Pradesh (NW India): phase equilibria versus thermobarometry. Schweizerische Mineralogische und Petrographische Mitteilungen 78, 107–132.

Vannay, J-C., Hodges, K.V., 1996. Tectonometamorphic evolution of the Himalayan metamorphic core between Annapurna and Dhaulagiri, central Nepal. Journal of Metamorphic Geology 14, 635–656.

Yeats, R.S., Nakata, T., Farah, A., Fort, M., Mirza, M.A., Pandey, M.R., Stein, R.S., 1992. The Himalayan Frontal Fault System. Annales Tectonicae 6, 85–98.

Zhao, W., Nelson, K.D., 1993. Project INDEPTH, 1993. Deep seismic reflection evidence for continental underthrusting beneath southern Tibet. Nature 366, 557–559.